# Multi-century impacts of ice sheet retreat on sea level and ocean tides in Hudson Bay

Hayden, Anna-Mireille; Gomez, Natalya; Wilmes, Sophie-Berenice; Green, Mattias

## Journal of Geophysical Research: Oceans

Published: 01/11/2020

Peer reviewed version

Cyswllt i'r cyhoeddiad / Link to publication

24. Oct. 2024

1    **Multi-century impacts of ice sheet retreat on sea level and ocean tides in Hudson Bay**

2

3    **Authors: A.-M. Hayden[1][*], S.-B. Wilmes[2], N. Gomez[1], J.A.M Green[2], L. Pan[1], H. Han[1], and**
4    **N.R. Golledge[3]**

5    [1]Department of Earth and Planetary Sciences, McGill University, Montreal, QC, Canada

6    [2]School of Ocean Sciences, Bangor University, Menai Bridge, Gwynedd, United Kingdom

7    [3]Antarctic Research Centre, Victoria University of Wellington, Wellington 6140, New Zealand

8    Corresponding author: Anna-Mireilla Hayden (anna-mireilla.hayden@mail.mcgill.ca)

9    *now at: Department of Geography and Environmental Management, University of Waterloo,
10   Waterloo, ON, Canada

11   **Key Points:**

12   - We model future sea level and tide changes in Hudson Bay, Canada due to continental ice
13     loss from past and present ice sheets.
14   - The magnitude and sign of future sea level and tide changes in Hudson Bay depend on
15     the evolution of the Antarctic Ice Sheet.
16   - Water depths in Hudson Bay could increase by 14.5 meters by 2500 if the Antarctic Ice
17     Sheet undergoes rapid retreat.

**Abstract**

18

19　Past and modern large-scale ice sheet loss results in geographically variable sea level changes.
20　At present, in Hudson Bay, Canada, sea level is decreasing due to glacial isostatic adjustment,
21　which represents a departure from the globally averaged sea level rise. However, there are large
22　uncertainties in future sea level trends with further polar ice sheet retreat in the coming centuries.
23　Sea level changes affect ocean tides considerably because tides are highly sensitive to changes in
24　bathymetry. Here, we present multi-century sea level projections associated with a suite of past
25　and future ice loss scenarios and consider the impact of these changes on ocean tides using an
26　established tidal model. Modern tides in Hudson Bay are poorly resolved due to large
27　uncertainties in bathymetry. To establish an initial condition for our simulations, we constrain
28　bathymetry in the bay using tide observations. Due to gravitational, Earth rotational and
29　deformational effects, Greenland ice loss will produce a small sea level fall in the bay, while
30　Antarctic ice loss will produce a larger than average sea level rise. Our results show that the
31　response of the Antarctic Ice Sheet to climate change strongly impacts the magnitude and sign of
32　future sea level and tidal amplitude changes in the region, with the largest changes predicted in
33　Hudson Strait and Foxe Basin. We emphasize that further constraints on bathymetry and accurate
34　projections of sea level and tides in Hudson Bay are imperative for assessing the associated
35　impacts on coastal communities and ecosystems.

36

**Plain Language Summary**

37

38　Hudson Bay is a shallow bay in northern Canada surrounded by coastal communities and
39　ecosystems that are vulnerable to future sea level change. The bay was ice covered 21,000 years
40　ago, and sea level is currently falling there due to ongoing land uplift since the ice retreated. It is
41　unclear if this trend will continue as the Greenland and Antarctic Ice Sheets melt, contributing to
42　spatially variable sea level changes. Sea level changes also impact ocean tides due to their
43　sensitivity to water depth. We model future sea level and tide changes in the Hudson Bay region
44　associated with land uplift and projections of Greenland and Antarctic ice loss over the next 500
45　years. With less Antarctic ice loss, sea level continues to fall and tidal amplitudes decrease.
46　Conversely, high-end projected Antarctic ice loss could increase water depths in Hudson Bay by
47　up to 14.5 meters by 2500 and tidal amplitude changes could exceed 1 meter, increasing in much
48　of Hudson Bay while decreasing in Hudson Strait. A better understanding of the response of
49　Antarctica to climate change will improve projections of sea level and tide changes in the Arctic
50　and the associated societal and environmental impacts.

**1. Introduction**

52　　　　Global mean sea level rise has accelerated in recent decades (Chen et al., 2017; Hay et
53　al., 2015; Nerem et al., 2018), and this acceleration is expected to continue as global
54　temperatures rise, resulting in thermal expansion of the oceans and melting of mountain glaciers
55　and the polar ice sheets (Church et al., 2013; Clark et al., 2015; Slangen et al., 2016). Of these
56　contributors, the Greenland and Antarctic Ice Sheets hold the largest potential to increase global
57　mean sea level (WRCP Sea Level Working Group, 2018), and are expected to be the dominant
58　contributors to global mean sea level rise on multi-century timescales (Church et al., 2013;
59　Golledge et al., 2015). Regional sea level changes associated with ice loss can differ
60　substantially from the global mean, due to gravitational, Earth deformational, and rotational

61 effects (e.g. Clark & Lingle, 1977; Gomez et al., 2010; Mitrovica et al., 2001). Furthermore, past
62 (ice age) ice cover changes lead to ongoing glacial isostatic adjustment (GIA) that contributes to
63 regional variability in sea level change. GIA effects can be considerable in regions such as the
64 Hudson Bay Complex (HBC, defined here as Hudson Bay, James Bay, Foxe Basin and Hudson
65 Strait, Figure 1a) in northern Canada that were once ice covered during the Last Glacial
66 Maximum. In the HBC, sea level is presently falling due to GIA, but it is unclear if this trend
67 will continue in the coming centuries due to the large uncertainties in the future evolution of the
68 polar ice sheets, in particular the Antarctic Ice Sheet (e.g. Church et al., 2013; DeConto &
69 Pollard, 2016; Golledge et al., 2015).
70 　　　Here, we define sea level as the height of the sea surface relative to the solid Earth
71 surface, or equivalently, ocean bathymetry. Global and regional patterns of sea level change have
72 been shown to have a strong influence on ocean tides (e.g., Padman et al. 2018; Wilmes et al.,
73 2017), because tides travel as shallow water waves, which are sensitive to ocean bathymetry.
74 Changes in ocean bathymetry (caused by changes in sea surface height and/or the shape of the
75 sea floor) can lead to changes in tidal wave propagation speed, energy dissipation, and
76 amplitudes (Green, 2010). Variations in sea level and the associated changes in ocean tides can,
77 in turn, affect other coastal processes and ecosystems such as the development of salt marshes,
78 coastal erosion, frequency and magnitude of flood events, and saltwater intrusion of surface
79 water (Craft et al., 2009; Kirwan & Guntenspergen, 2010; Kirwan et al., 2010; Kirwan &
80 Megonigal, 2013; Nicholls & Cazenave, 2010; Ross et al., 2017). Finally, Arctic and sub-Arctic
81 indigenous communities surrounding the HBC are among the most vulnerable to climate change
82 (IPCC, 2014), with their livelihoods and food sources critically impacted by coastal changes (e.g.
83 Lemmen et al., 2016; Tsuji et al., 2009, 2016).
84 　　　Projections of future sea level change in the HBC due to climate change have been
85 relatively limited. Gough (1998) suggested that sea level in Hudson Bay could begin to increase
86 in the current century as the global mean sea level rise associated with climate change outpaces
87 the sea level fall due to glacial isostatic uplift. However, Gough's simple model did not capture
88 the spatial variability in sea level change that arises from melting current ice sheets. More
89 recently, Tsuji et al. (2009, 2016) and Lemmen et al. (2016) calculated the spatially variable sea
90 level change and suggested that glacial isostatic uplift would persist in parts of the HBC in the
91 coming centuries but did not consider a wide range of possible climate-driven sea level changes.
92 Recent work has shown that even under the same climate forcing scenario, Representative
93 Concentration Pathway (RCP) 8.5, projections of Antarctica's contribution to global mean sea
94 level rise range from 2.25 m to 15.65 m by 2500 (DeConto & Pollard, 2016; Golledge et al.,
95 2015, 2019). Given this large uncertainty, it is unclear what the dominant contributor to sea level
96 change in the HBC will be, or even what the sign of sea level change will be. Furthermore, due
97 to the relatively shallow bathymetry in the HBC, and the low-lying topography that surrounds
98 the bay (Figure 1a), a small rise or fall in sea level will result in a large shoreline migration,
99 amplifying the HBC's sensitivity to uncertainty in future sea level change.
100 　　　Previous regional studies have investigated future sea level and tide changes on the
101 European Shelf (e.g., Idier et al., 2017; Pelling & Green, 2014; Pickering et al., 2012), the
102 Patagonian Shelf (Carless et al., 2016), the Gulf of Maine (Pelling & Green, 2013), the Gulf of
103 Mexico (Passeri et al., 2016), and the Bohai Sea in China (Pelling et al., 2013), but studies of the
104 HBC are lacking. The HBC is a particularly interesting region with regards to ocean tides. The
105 tidal range of Ungava Bay in Hudson Strait (16.8 m ± 0.2 m, Drinkwater, 1986), rivals that of the
106 Bay of Fundy (17.0 m ± 0.2 m, O'Reilly et al., 2005), as the region with the largest tidal range in

107  the world. Furthermore, Egbert & Ray (2001) found that more tidal energy is dissipated in the
108  HBC alone than in any other region in the world. This is because the HBC is near resonant at the
109  semi-diurnal tidal forcing frequency (Arbic et al., 2007; Webb, 2014), producing large semi-
110  diurnal tides (exceeding 4 m amplitudes in some areas, Figure 1b) that are further amplified due
111  to the HBC's location on a continental shelf (Clarke & Battisti, 1981). The resonant properties of
112  the HBC and its shallow continental shelf sea character can strongly influence deep ocean tides
113  in the connecting Atlantic Ocean (Arbic et al., 2009; Arbic & Garrett, 2010), so any large-scale
114  change in the HBC can have consequences far away from the region. Previous work on
115  paleotides in the region indicated a strong sensitivity of ocean tides to changes in sea level (Arbic
116  et al., 2004; Egbert et al., 2004; Uehara et al., 2006). However, modern tides in the HBC are not
117  well resolved due to limited bathymetry data that can be used to constrain models (Egbert &
118  Ray, 2001). Projecting future tides therefore requires, as a first step, an appraisal of the
119  performance of available bathymetry models in reproducing modern tides in the HBC.
120      Wilmes et al. (2017) showed that a future complete collapse of the Greenland and West
121  Antarctic ice sheets would strongly impact tides globally, and that simulations that take into
122  account spatial variability in sea level change differ substantially from those that assume the
123  global average equivalent rise. In particular, in Hudson Bay, the spatially variable sea level
124  change associated with Greenland ice loss is opposite in sign to the uniform global average sea
125  level rise scenario, which, in turn, results in large differences in predicted tidal changes.
126  Furthermore, they show that spatially variable changes in sea level, and in turn tidal amplitudes
127  in much of the HBC are positive under West Antarctic ice sheet collapse and negative under
128  Greenland ice sheet collapse.
129      As a complete collapse of the Greenland and West Antarctic ice sheets represents a long
130  term, upper bound on their contribution to sea level change, a question arises: How will future
131  sea level and tides in the HBC evolve under combined, transient melting of the ice sheets in the
132  coming centuries? Greenland's contribution to sea level change, which is not expected to exceed
133  20 cm of global mean sea level equivalent by 2100 (Church et al., 2013; IPCC, 2019), is
134  predominantly driven by surface mass balance, followed by ice discharge via icebergs (Church et
135  al., 2013; IPCC, 2019). The HBC is relatively insensitive to Greenland ice loss due to its close
136  proximity to the net-zero sea level change line associated with gravitational effects that arise
137  from Greenland melting. Conversely, the dynamic response is expected to dominate sea level
138  changes due to Antarctic ice loss, but the future contribution from Antarctica remains highly
139  uncertain due to the lack of observations to constrain models and an incomplete description of
140  ice sheet-ocean-atmosphere interactions in current models (Kopp et al. 2017; IPCC, 2019).
141  Projections range from tens of centimeters to more than 10 m global mean sea level equivalent
142  over multi-century timescales (e.g., Golledge et al., 2019; Pollard et al., 2017). In contrast to
143  Greenland melting, gravitational effects due to Antarctic ice loss will lead to a larger-than-
144  global-average sea level rise in the HBC. Here, we investigate to the opposing influence of
145  gravitational effects and the large uncertainty in Antarctic projections on sea level and tide
146  changes in the HBC. We consider a single contribution from the Greenland Ice Sheet and low-
147  and high-end possible contributions to sea level change from the Antarctic Ice Sheet under
148  RCP8.5 climate warming. On decadal timescales, sea level changes will likely be dominated by
149  GIA, but on centennial timescales, the contribution from ice sheets could exceed GIA, in
150  particular under high-end warming scenarios. This transition from a regime of sea level fall to
151  one of rise, and the associated changes in tides, is important to consider in assessing coastal
152  climate change impacts and develop adaption strategies.

153         The paper is structured as follows. In section 2, we describe the ice loss and sea level
154 projections and the tide model setup. Due to the sensitivity of tides to bathymetry, we discuss
155 constraints on modern bathymetry in the HBC in section 3 and present a bathymetry model that
156 improves modern non-assimilative tide simulations. In section 4, we present predictions of future
157 sea level changes associated with future retreat of the polar ice sheets and ongoing GIA and the
158 associated tidal changes in the HBC. We conclude with a discussion in section 5.
159
160    **2. Methods**

161 *2.1 Sea level and ice sheet modelling*
162         We adopt the sea level theory from Kendall et al. (2005) and Gomez et al. (2010) to
163 predict the spatially variable sea level changes resulting from past and future ice cover variations
164 using a gravitationally self-consistent sea level model that incorporates viscoelastic deformation
165 of the solid earth due to surface ice and ocean mass loading, migrating shorelines, and Earth
166 rotational effects. Elastic and density structure of the solid Earth in all simulations is provided by
167 the Preliminary Reference Earth Model (PREM) (Dziewonski & Anderson, 1981) and viscosity
168 structure is given by the VM2 Earth model (Peltier, 2004) unless otherwise specified. The
169 modern topography that serves as input to the sea level model is taken from GEBCO 2014
170 (Weatherall et al., 2015) globally, with the composite regional bathymetry described below over
171 the HBC. All calculations are performed up to spherical harmonic degree 512.
172         We simulate the future evolution of the polar ice sheets in Greenland and Antarctica with
173 dynamic ice sheet models. We focus on projections adopting RCP 8.5 (Collins et al., 2013),
174 representing the business-as-usual emissions scenario as it serves as the upper bound of expected
175 global temperature increase, and hence contribution of the ice sheets to sea level change in the
176 HBC. Furthermore, by considering a single RCP scenario, we highlight the variability that
177 emerges among ice loss and sea level projections that are guided by the same emissions
178 framework.
179         Greenland and Antarctic ice thickness projections are generated using the Parallel Ice
180 Sheet Model (PISM) version 0.7.3, a hybrid ice model with shallow shelf-shallow ice
181 approximations for floating and grounded ice (Winkelmann et al., 2011). Following the
182 procedure outlined in Golledge et al. (2019), future climate forcing on the ice sheets is driven by
183 the Coupled Model Inter-comparison Project Phase 5 (CMIP5) multi-model ensemble mean
184 outputs. The ice sheet model simulations are performed on a high-resolution (2.5 km for
185 Greenland and 5 km for Antarctica) polar stereographic grid. We apply a Gaussian smoothing
186 filter on the changes in total (floating and grounded) ice thicknesses, then interpolate ice
187 thickness predictions onto a lower resolution Gauss-Legendre 512 x 1024 global grid, to serve as
188 input to the sea level model. We consider the Antarctic projection from Golledge et al. (2019) as
189 the low-end projection of future Antarctic ice loss under RCP8.5 (henceforth the "low-end"
190 scenario). We also consider an alternative simulation for the Antarctic Ice Sheet that predicts
191 much greater ice loss under RCP8.5. This high-end projection of Antarctic ice thickness changes
192 (hereafter referred to as the "high-end" scenario) is provided by a simulation in Pollard et al.
193 (2017) using a coupled ice sheet – sea level model that includes ice cliff and hydrofracturing
194 physics and a hybrid combination of shallow ice-shallow shelf approximations for ice dynamics.
195 Ice thickness variations are provided by the ice model at 20 km resolution and then linearly
196 interpolated onto the global 512 x 1024 grid.
197         To fully quantify the sea level changes in Hudson Bay, we also incorporate the
198 contribution of ongoing GIA associated with past ice cover changes over the last deglaciation,

199  which, in our simulations, spans the time period of 21,000 years ago to the year 2000 (henceforth
200  the modern). We model ice loading changes over the last deglaciation by adopting the ICE-5G
201  ice history with the VM2 Earth model (Peltier, 2004) and the ICE-6G ice history with the VM5a
202  Earth model (Argus et al., 2014; Peltier et al., 2015). Each simulation was run from 21,000 years
203  ago to 500 years in the future, and the predictions of change from the modern to the year 2500
204  were added to the sea level changes associated with future ice sheet retreat described above (see
205  Figure S1 for a comparison of ICE-5G and ICE-6G).
206       The total sea level change is calculated as the sum of the contributions from Greenland,
207  Antarctica, and GIA. Note that our projections do not include oceanographic effects. In the
208  current century, these are expected to contribute a relatively uniform sea level rise in the bay
209  under future climate warming (Jevrejeva et al., 2016), but the magnitude, timing and spatial
210  variability of these changes is challenging to simulate in the HBC on multi-century timescales.
211  While these effects would alter the timing of the change from a sea level fall to a sea level rise,
212  they would likely not offset the overall effect of transitioning from a sea level fall to a sea level
213  rise. In addition, the size of the contribution is well within the range of Antarctic contributions
214  considered here. Shorter timescale simulations should include the influence of ocean dynamics
215  on sea level and tides.
216
217  *2.2 Tide modelling*
218       We use the Oregon State University Tidal Inversion Software (OTIS) (Egbert et al.,
219  1994; 2004) to model present-day and future tides in Hudson Bay. OTIS solves the linearized
220  shallow water equations forced by the tidal potential and with energy dissipation from bed
221  friction and parameterized tidal conversion (e.g., Green & Nycander 2013; see Wilmes et al.,
222  2017 for details on the model setup).
223       The HBC tide model was run at $1/30°$ x $1/30°$ horizontal resolution and simulated the
224  tidal constituents $M_2$, $S_2$, and $K_1$. The extent of the model domain is shown in Figure 1.
225  Dissipation of tidal energy was calculated according to Egbert and Ray (2001; see also Wilmes
226  et al., 2017 for a detailed description). For the present-day simulations, TPXO8 (Egbert &
227  Erofeeva, 2002; see http://volkov.oce.orst.edu/tides/tpxo8_atlas.html for the latest version)
228  elevations were used as forcing at the open boundaries. TPXO8 is an observation constrained
229  tide model solution that assimilates tide gauge observations and satellite altimetry to produce a
230  highly accurate estimate of the tides (~2 cm RMS error compared to un-assimilated tide gauge
231  data; see Egbert & Erofeeva, 2002, and Stammer et al., 2014 for details).
232       For the future tide simulations, sea level change predictions described in section 2.1 are
233  added to the present-day bathymetries for both HBC and the global setup. Simulations are
234  performed for 2100, 2300, and 2500 under low-end and high-end Antarctic contributions.
235  Elevation changes in response to each of the future sea level change scenarios simulated by a
236  near-global (86° S - 89° N) tidal model (see next paragraph) were added to the boundary
237  conditions used for the present-day simulations, thereby ensuring a high degree of accuracy for
238  high-resolution HBC future simulations. We carry out two sets of runs for each time slice: one
239  where flooding of low-lying land is permitted (denoted 'flood') and a second one where flooding
240  is not permitted ('no-flood').
241       The near-global tide model simulations were also run with OTIS (see Wilmes et al., 2017
242  for details on linearized shallow wave equations, and internal drag and SAL parameterizations).
243  The underlying bathymetry is RTopo-2 (Schaeffer et al., 2016) and the model is run at $1/8°$ x
244  $1/8°$ horizontal resolution for 21 days to simulate $M_2$, $S_2$ and $K_1$. The $M_2$ amplitude errors when

245  compared to TXPO8 are 5.6 cm globally and 2.8 cm in the deep ocean (see Table S1). Integrated
246  $M_2$ tidal dissipation for the global and deep ocean is within 6 % and 7 %, respectively, of values
247  computed for TPXO8, despite the very different resolutions in the shelf seas (TXPO8 has a
248  resolution of 1/30 degree in most shelf seas; see also Egbert and Ray, 2001). Simulations using
249  the same sea level scenarios as for the regional model were carried out with the near-global
250  model and used as boundary conditions for the regional model simulations. Land-ocean
251  boundaries in this case were kept constant (i.e., land was not permitted to flood) due to the low
252  resolution of the model.
253

254  ### 3.  Constraining Modern Bathymetry

255       Numerical prediction of tides in near-resonant basins, such as Hudson Bay, are strongly
256  sensitive to the adopted ocean bathymetry (Egbert & Ray, 2001; Green, 2010; Padman et al.
257  2018). Therefore, in order to project future tide changes, we require an accurate estimate of
258  modern bathymetry. Bathymetry in the HBC is poorly constrained due to the sparsity of
259  available data, related to the HBC's shallow depths, spatial extent, and limited commercial
260  shipping routes. Furthermore, there is substantial disagreement between global bathymetry
261  datasets in the HBC (Figure S2); differences between datasets reach up to 200 m in some areas
262  of the complex. As a result, tide models struggle to accurately capture the tides in the region.
263       Given the lack of available data to distinguish between these bathymetry models, we seek
264  to simultaneously find a bathymetry to use for (future) projections and to improve non-
265  assimilative modelling of the modern tides in HBC. To do this, we simulate modern tides in the
266  HBC using the configuration described in 2.2 with a suite of different bathymetry models
267  GEBCO 2008 (see The GEBCO_2008 Grid, version 20100927, www.gebco.net), GEBCO 2014
268  (Weatherall et al., 2015), ETOPO1 (Amante & Eakins, 2009), and SRTM30_Plus (Becker et al.,
269  2009) and evaluate their performance, focusing on Hudson Bay and Strait.
270       Figure 2a-d shows the difference between the simulated $M_2$ tidal amplitudes using the
271  four bathymetry datasets considered (ETOPO1, GEBCO 2008, SRTM30_Plus, and GEBCO
272  2014) and the TPXO8 amplitudes. We calculate the root mean square complex elevation errors
273  (RMSEs) against 14 tide gauges (see Text S1 for details and Figure 2 for their locations),
274  TPXO8 and TPXO9 (see https://www.tpxo.net/global/tpxo9-atlas for details and the latest
275  version) to evaluate the performance of bathymetry models in reproducing modern tides over the
276  global domain (see Table 1 for a quantification of the errors). Amplitude and phase RMSEs are
277  shown in Tables S2 and S3 for all ocean depths (total RMSE) and deep oceans regions (water
278  depths > 500 m, deep RMSE).
279       The simulation using ETOPO1 produced the largest elevation and amplitude errors of all
280  the simulations (Figure 2a and Table 1), with amplitudes differing from TPXO8 by more than 1
281  m in Hudson Strait and James Bay. Both GEBCO 2008 (Figure 2b) and GEBCO 2014 (Figure
282  2d) perform well in Hudson Strait, each with mean amplitude differences of 21 cm and 15 cm in
283  Hudson Strait, respectively. In Hudson Bay, SRTM30_Plus (Figure 2c) matches more closely
284  than the GEBCO simulations, differing from TPX08 with a basin amplitude RMSE of 7 cm. The
285  largest amplitude errors in all simulations are in Hudson Strait, where there are also the largest
286  differences in depths between datasets (Figure S2) and the largest tidal amplitudes (Figure 1b).
287       To improve the accuracy of our non-assimilative tidal simulations, we develop a
288  composite bathymetry (Figure 2e) based on how well each existing bathymetry dataset
289  performed regionally in the comparison to TPXO8 in the HBC. Our composite bathymetry
290  merges, using linear weighting, SRTM30_Plus bathymetry in Hudson Bay and GEBCO 2008

291  bathymetry elsewhere in the HBC. The amplitudes of the tide simulation adopting the composite
292  bathymetry differ from TPX08 in Hudson Bay on average by 6 cm. The largest amplitude errors
293  in James Bay and Foxe Basin are less than ± 25 cm, with mean errors of 5 cm and 13 cm,
294  respectively. Our composite bathymetry improves the amplitude fit in Hudson Strait, with an
295  average amplitude difference of 20 cm when compared to TPXO8. Furthermore, we find that our
296  composite, regional bathymetry substantially reduces elevation errors both in comparison to tide
297  gauges, TXPO8 and TXPO9 (Table 1) and also both total and deep RMSE for amplitudes and
298  phases ( Table S3) for all simulated constituents. Consequently, we adopt this composite, modern
299  bathymetry in the future sea level and tide projections shown in the sections to follow.
300

## 4. Results

*4.1 Sea level change*

303  Figure 3 shows the projected contributions to sea level change in the HBC associated
304  with GIA and melting from the Greenland Ice Sheet and Antarctic Ice Sheet for the three time
305  slices 2100, 2300 and 2500. The contribution from GIA (Figure 3a-c) shows a sea level fall
306  across the HBC. James Bay and Churchill, Manitoba regions experience the maximum predicted
307  sea level fall (see Figure 1a), with a magnitude of 1.2 m in both regions by 2100, and 5.9 m and
308  5.7 m respectively, by 2500. In Foxe Basin, sea level fall associated with GIA reaches 0.9 m by
309  2100, and 4.3 m by 2500. The sea level fall is driven by the larger thickness of the Laurentide Ice
310  Sheet during the Last Glacial Maximum in these regions and the later termination of
311  deglaciation. Hudson Strait sees a more moderate fall of 0.3 m by 2100 and 1.5 m by 2500. In
312  contrast, to the east of the HBC in Davis Strait region, sea level rises over the 500-year GIA
313  simulation (red regions in Figure 3a-c) due to the subsidence of peripheral bulges that formed
314  around the ice sheets at the Last Glacial Maximum in our ICE-5G simulation.
315  Next, we consider the contribution from melting of the polar ice sheets (Figure 3d-l).
316  There are a number of physical effects contributing to the differences in sea level change in the
317  HBC associated with Greenland (Figure 3d-f) and Antarctic (Figure 3g-l) ice loss. An ice sheet
318  exerts a gravitational attraction on the surrounding water, and this attraction weakens as the ice
319  sheet loses mass, resulting in a local sea level fall within ~2000 km of the ice loss (Woodward,
320  1888). At greater distances from the source of ice loss, sea level rises more the global average
321  (Tamisiea & Mitrovica, 2011). Viscoelastic uplift of the solid Earth in and around the region of
322  ice loss further accentuates the local sea level fall, and deformation of the Earth due to loading of
323  the oceans with water and changes in the planet's rotation associated with surface mass
324  redistribution add geographic variability to the sea level change farther away from the ice sheet.
325  In our simulations, the Greenland Ice Sheet is projected to contribute 0.10 m and 0.55 m of
326  global averaged sea level rise by 2100 and 2500, respectively, but the HBC is within the zone of
327  gravity-driven sea level fall for the Greenland Ice Sheet. Therefore, Greenland melting is
328  projected to contribute a low amplitude drop in sea level across the HBC that decreases in
329  amplitude with distance from Greenland. The smallest sea level decrease occurs in the south-
330  eastern part of the HBC (Figure 3d-f and Figure S3a) and the largest sea level fall can be seen in
331  northern Foxe Basin (up to 0.7 m by 2500) and the northern Labrador Sea. In Hudson Strait, the
332  projected sea level decrease reaches 0.5 m by 2500. Central Hudson Bay would experience up to
333  a 0.2 m decrease in sea level by 2500. In James Bay, sea level remains unaltered by 2100, with a
334  shift to a sea level rise by 2500 that does not exceed 0.10 m. The sea level fall due to Greenland
335  melting is an order of magnitude smaller than that caused by GIA. Sea level in the HBC is hence

336 relatively insensitive to Greenland ice loss due to the fingerprint pattern and the proximity of the
337 southern and western coasts of the HBC to the region of net-zero sea level change.
338      Melting from the Antarctic Ice Sheet, on the other hand, would lead to a sea level rise in
339 the HBC that is approximately 1.2 times greater than the global mean sea level equivalent rise
340 associated with the melting, with a relatively uniform rise across the HBC ( Figure S3b). Figure
341 3g-l show projected sea level changes in response to the low-end (Figure 3g-i) and high-end
342 (Figure 3j-l) responses of the Antarctic Ice Sheet to the RCP8.5 scenario. Under the low-end
343 simulation, Antarctic melting would lead to a maximum sea level rise in the HBC of 0.1 m by
344 2100 and 2.1 m by 2500. The high-end scenario (j-l) predicts an order of magnitude larger sea
345 level rise of up to 0.8 m by 2100 and 14.5 m by 2500 across the HBC.
346      In Figure 4, we consider the sum of all the contributions shown in Figure 3 (see also
347 Figure S4 for the total sea level change adopting ICE-6G). Under the low-end Antarctic ice loss
348 scenario (Figure 4a-c), the sea level change at 2100, 2300, and 2500 is dominated by GIA
349 effects. The largest sea level decreases are predicted in the regions where the signal from GIA is
350 greatest (Figure 3a-c). At 2100 (Figure 4a), the magnitude of sea level fall ranges from 1.1 m in
351 Churchill to 1.2 m in James Bay. In Hudson Strait, the amplitude of sea level fall is damped and
352 on the order of 0.4 m. East of Hudson Strait in the Davis Strait, a slight rise is seen, where
353 Antarctic ice loss and GIA are both contributing a sea level rise. By 2300 (Figure 4b), the sea
354 level fall ranges from 1 m in central Hudson Bay up to 2.75 m in James Bay. Ungava Bay, at the
355 entrance of Hudson Strait, is the only area in the HBC that experiences a sea level rise, reaching
356 up to 0.4 m. Thus, despite that the largest sea level fall due to Greenland ice loss is predicted in
357 the Hudson Strait (Figure 3d-f), in addition to the contribution from GIA, the rise associated with
358 Antarctic ice loss is not compensated for. By 2500, the sea level fall across much of the HBC
359 reaches 3 m. Our low-end simulation suggests a gradual extension of sea level rise into the HBC.
360 By 2500, the extent of sea level rise spreads westwards from the Hudson Strait into Hudson Bay,
361 where sea level rise is less than 0.5 m.
362      The projection that incorporates the high-end Antarctic scenario is characterized by a
363 transition from sea level fall to sea level rise across the HBC over the simulation time. At 2100
364 under this high-end Antarctic scenario (Figure 4d), GIA still dominates in Hudson Bay, James
365 Bay and northern Foxe Basin. In other regions of the HBC, the signal of sea level rise from
366 Antarctic ice loss already begins to outpace the signal from GIA by 2100. We find that by 2200
367 sea level has begun to rise across the entire HBC. Despite the large GIA signal in Foxe Basin and
368 James Bay, our projections indicate that these regions would experience up to 3 m of sea level
369 rise by 2200 and that sea level rise in other regions in the HBC reaches up to 4.5 m. In 2300
370 (Figure 4e), a maximum sea level rise of 9.5 m is predicted in Ungava Bay in Hudson Strait, with
371 the smallest rise of 6.3 m in James Bay. The magnitude of minimum sea level rise under the
372 high-end scenario at 2300 is triple the magnitude of maximum sea level fall predicted from the
373 low-end scenario. At 2500 (Figure 4f), sea level rise exceeds 14 m in some regions of Hudson
374 Strait. In Foxe Basin, the projected 10 m rise by 2500 represents, on average, a 10 % increase in
375 water depth, relative to present day. Moreover, the 9 m rise predicted for James Bay suggests a
376 20 % increase in water depth relative to present day. As in 2300, we find that the magnitude of
377 minimum sea level rise in James Bay and Foxe Basin under the high-end scenario in 2500 is
378 three times the magnitude of maximum sea level fall calculated from the low-end scenario.
379
380 *4.2 Tides*

381   In Figure 5, we present the $M_2$ tidal amplitude changes associated with the total sea level
382 changes shown in Figure 4. The tidal $M_2$ amplitude responses differ substantially between the
383 low-end (Figure 4a-c) and high-end (Figure 4d-e) Antarctic ice loss scenarios. For the low-end
384 scenarios, all three time slices show a similar amplitude change pattern with changes increasing
385 in magnitude from 2100 to 2500. Both the flood (Figure 5) and no-flood (Figure S8) runs show
386 very similar amplitude change characteristics, therefore the description will be based on the
387 simulations permitting flooding. Amplitudes increase in Hudson Strait and in the western half of
388 Foxe Basin whereas decreases can be seen along most of the Hudson Bay margins.
389   Under the low-end scenario and in Foxe Basin, where sea level deceases by ~1 m in 2100
390 and by over 2 m in 2300 and 2500, respectively, occur, the amphidrome in the eastern part of the
391 bay is shifted eastward due to increases in the energy fluxes into the eastern part of the bay (see
392 panels a-c in Figures S9 and S10). Small decreases in the energy fluxes along the western margin
393 of Hudson Bay can be seen which are associated with a small shift of the western amphidrome
394 towards the western margin, thus decreasing amplitudes. The eastern amphidrome shifts north-
395 eastward leading to deceases in amplitudes along the eastern margin. In James Bay, the
396 amphidrome in the east moves eastward and becomes degenerate, leading to increases in
397 amplitudes in the south-east part of the bay.
398   For the simulations adopting the high-end Antarctic ice loss scenario, the changes for the
399 2100 simulation are small and will therefore not be discussed. For the 2300 and 2500 high-end
400 scenarios (as in the low-end scenarios), the flood and no-flood responses are very similar.
401 However, in the no-flood simulations the amplitude changes are larger, especially along the
402 eastern margins of Hudson Bay and Foxe Basin (see Figure S8). In the flood runs, for both 2300
403 and 2500 (see panels e and f in Figures 5 and S8), large amplitude decreases can be seen in
404 Hudson Strait (exceeding 70 cm by 2500), in Ungava Bay and in the southern and northern parts
405 of Foxe Basin (exceeding 1 m by 2500 in both regions). In eastern Foxe Basin and along the
406 eastern margins of Hudson Bay, amplitudes increase by around 20-30 cm by 2500, whereas
407 along the south-eastern margins of Hudson Bay amplitudes decrease by approximately the same
408 amount.
409   The amplitude decreases in Hudson Strait for 2300 and 2500 high-end Antarctic ice loss
410 scenarios exceed 25 % and are associated with a strong decrease in energy fluxes through
411 Hudson Strait and into Foxe Basin (see panels e and f in Figures S9 and S10). The decrease in
412 energy fluxes together with increases in energy losses in the newly flooded areas around the
413 margins of Foxe Basin shift the eastern amphidrome in Foxe Basin southward, thus increasing
414 amplitudes in the easternmost part of the basin and decreasing amplitudes in the south. Similarly,
415 energy fluxes along the western margins of Hudson Bay decrease, shifting both amphidromes
416 westward and increasing amplitudes in the east of the bay. In James Bay, the decreased energy
417 flux shifts the amphidrome north-westward increasing amplitudes in the south east of the bay and
418 leading to decreases in the western half.
419   Next we consider the impact on energy dissipation. For the low-end simulations,
420 integrated dissipation over the area of HBC remains similar to present (Table S8). In the no-flood
421 runs, dissipation remains constant at the present-day value of 232 GW with increases and
422 decreases in Foxe Basin cancelling each other out in all three time-slices. In the flood runs, total
423 dissipation increases by 5 % in the 2500 time slice. For the high-end scenarios, in contrast, the
424 changes are much larger. In the no-flood runs, integrated dissipation of the HBC decreases by 23
425 % by 2300 and 40 % by 2500. Nearly all of the decreases in dissipation are due to reduced
426 energy losses in Foxe Basin, Hudson Strait and Ungava Bay. In the 2500 time-slice, these three

427 areas together experience a drop in dissipation of ~80 GW which explains the majority of the
428 dissipation decrease. For the flood runs, the dissipation change picture is very similar (see panels
429 e and f in Figures S11 and S12), however, the integrated dissipation changes by only 3 and 7 %
430 for 2300 and 2500, respectively. In these runs, the energy losses in the newly flooded areas
431 nearly balance the dissipation losses away from the margins. However, if the newly flooded
432 areas are excluded, the same large dissipation decreases in the three basins emerge (see last two
433 columns of Table S8).
434
435 ### 5. Discussion and Conclusions
436 We have provided the first regional study of future sea level changes in the Hudson Bay
437 associated with ice loss from the Greenland and Antarctic Ice Sheets and GIA and their impact
438 on ocean tides in the region. We showed that both sea level and tides in the HBC are relatively
439 insensitive to Greenland melting but strongly sensitive to Antarctic Ice Sheet evolution, with our
440 simulations indicating a transition from a sea level fall to a sea level rise across the HBC that is
441 dependent on the adopted Antarctic ice loss scenario. In this work, we focused on the RCP8.5
442 emissions pathway, however more moderate warming scenarios such as RCP2.6 or RCP4.5
443 could prolong the duration of sea level fall in the HBC.
444 Our results indicate that the sea level fall associated with GIA contributes significantly to
445 sea level change in the HBC and dominates under low-end Antarctic ice loss scenarios. HBC is
446 dominated by sea level decreases (up to 1.2 and 3 m by 2100 and 2500, respectively). Hudson
447 Strait is the only region that experiences sea level rise (up to 0.5 m by 2500). We found that the
448 associated $M_2$ tidal amplitude changes are less than 0.2 m in the HBC by 2500, with tidal
449 amplitude increases in Foxe Basin and western Hudson Strait, and tidal amplitude decreases
450 across Hudson Bay, James Bay, and Ungava Bay in Hudson Strait. We have shown that small
451 migrations of the amphidromic points are responsible for the observed changes in the $M_2$ tides.
452 Conversely, GIA does not compensate the projected sea level rise under more rapid
453 Antarctic ice loss in our high-end scenario. In the projection adopting the high-end Antarctic ice
454 loss scenario, sea levels begin to rise in much of the HBC by 2100, with a widespread transition
455 from sea level fall to sea level rise by 2200 and reaching a peak sea level rise of 14.5 m in
456 Ungava Bay in Hudson Strait by 2500. Under the high-end scenario, the $M_2$ tidal amplitude
457 changes reach over 1 m with the largest decreases occurring in Hudson Strait and Foxe Basin and
458 peak increases along the eastern margin of Hudson Bay by 2500. Furthermore, as the HBC is
459 presently one of the areas on the planet where the most tidal energy is dissipated (Egbert & Ray,
460 2001) the significant decreases in dissipation in the open ocean areas of Hudson Strait, Foxe
461 Basin and Ungava Bay (see panels d-f in Figures S11 and S12) suggested under our high-end
462 scenario simulations could affect both local tidal mixing important for biogeochemistry but also
463 the global tidal energy balance.
464 Our results suggest that the strong and uniform in sign responses of the Hudson Strait,
465 Ungava Bay and Foxe Basin system to the sea level variations in both the high-end and low-end
466 scenarios could be linked to the resonant properties of the basins. A number of previous studies
467 have shown that the HBC straddles a number of resonant frequencies close to and either side of
468 the $M_2$ frequency (Arbic et al., 2007, Cummins et al., 2010, and Webb, 2014). Our simulations
469 show that Hudson Strait, Ungava Bay and Foxe Basin change in conjunction with each other in
470 response to sea level changes. The moderate decreases in sea level (around 2 m) seen in the low-
471 end scenario lead to increases in amplitudes, suggesting that the system is moving closer to a
472 resonant state. In contrast, the increases in sea level seen in the high-end scenario in the 2300 and

473   2500 time slices drive strong amplitude decreases in Hudson Strait, Ungava Bay and Foxe Basin
474   together with large decreases in dissipation. In the 2500 high-end simulations (both flood and no-
475   flood), the dissipation decreases amount to around 80 GW when newly flooded areas are
476   excluded, nearly halving the energy dissipated in the three basins with respect to present day.
477       Previous studies investigating resonances have generally considered Hudson Strait and
478   Hudson Bay (together with Ungava Bay) as a resonant system (see e.g., Cummins et al., 2010).
479   However, our results indicate that it is more likely that Foxe Basin and Hudson Strait together
480   with Ungava Bay act as a near-resonant system at present; which, perturbed by sea level
481   changes, exhibits large changes in amplitudes and dissipation. At present, in Foxe Basin ~110
482   GW of M2 tidal energy are dissipated, whereas in Hudson Bay a mere 20 GW are lost (see also
483   Figure S13). Nearly half of the dissipation decreases in the 2500 high-end scenario occur in Foxe
484   Basin, and the remainder take place in Hudson Strait and Ungava Bay. This hypothesis is
485   supported by the pathway of the energy fluxes into the HBC (see Figure S14) and the changes
486   thereof ( Figures S9 and S10) (see also Figure 1 in Webb et al., 2014) where the main pathway of
487   energy flow into HBC is through Hudson Strait and into the eastern part of Foxe Basin with very
488   little energy transfer into Hudson Bay itself. A simple back of the envelope calculation of the
489   natural period of Hudson Strait and Foxe Basin ($T = 4L/\sqrt{gD}$), using a distance $L$ of 1600 km
490   from outside the entrance of Hudson Strait to the south eastern margin of Foxe Basin and a mean
491   depth $D$ of 136 m, yields a resonant period $T$ of 48.7 hrs, which is very close to four-times the
492   $M_2$ period. A sea level decrease by 2 m as seen in the 2300 and 2500 low-end simulations
493   increases the resonant period to 49.0 hrs, i.e. moving it closer to 4 times the $M_2$ period. In
494   contrast, a sea level increase of 9 m and 13 m as in the 2300 and 2500 high-end simulations
495   results in decreases in the resonant period to 47.1hrs and 46.5 hrs, respectively, thus moving
496   away from four times the $M_2$ period.
497       We have carried out additional simulations with the same sea level forcing across HBC
498   but with present-day boundary conditions at the open boundaries (not shown) and find very
499   similar results as when we apply boundary conditions from the global model forced with sea
500   level changes. A no-flood simulation of the high-end 2500 sea level change shows a dissipation
501   decrease of 35 % which is very similar to the 40 % seen in our no-flood runs. We therefore
502   conclude that, to a large extent, the changes seen in Hudson Bay, Ungava Bay and Foxe Basin
503   are driven by changes in internal dynamics due the sea level changes rather than by external
504   forcing outside our regional model domain. This is in contrast to, e.g., the work by Harker et al.
505   (2019) carried out for the Australian Shelf.
506       Our HBC tidal runs performed at 1/30° degree resolution are more accurate than the
507   global simulations shown in Wilmes et al. (2017) with a resolution of 1/8°. They found a global
508   RMS error for M2 amplitudes of 7.7 cm (global) and 3.8 cm (deep) whereas our new global
509   model setup has reduced errors of 5.6 cm (global) and 2.8 cm (deep). However, the responses to
510   sea level changes in their simulations are similar to our findings for the HBC simulations. They
511   compared tidal amplitude responses to non-uniform sea level changes due to full collapses of the
512   West Antarctic Ice Sheet and the Greenland Ice Sheet and a uniform sea level rise of 12 m. The
513   spatially variable sea level change scenario had a similar magnitude sea level fall over the HBC
514   as the 2500 low-end scenario whereas the uniform sea level rise case was most akin to the 2500
515   high-end case shown here. The amplitude responses to the two different scenarios agree in their
516   patterns between the two studies which increases our confidence in the results presented in
517   Wilmes et al. (2017), despite the different model resolutions.

518     Here, we focused on the contributions due to ice mass loss from the polar ice sheets and
519 GIA associated with the last deglaciation, however, oceanographic and sea ice changes in the
520 HBC will also impact sea level and ocean tides, in particular on timescales shorter than the
521 centennial timescales considered here. Thermal expansion and ocean dynamics are expected to
522 contribute on the order of 0.3 m of sea level rise in the HBC under RCP8.5 by 2100 (Jevrejeva et
523 al., 2016), similar to the contribution of these effects to globally averaged sea level rise of 0.21-
524 0.33 m by 2100 estimated in the IPCC (Church et al., 2013). While regional estimates in the
525 HBC are limited on multi-century timescales, the contribution of thermal expansion and ocean
526 dynamics to globally averaged sea level rise under RCP8.5 is estimated to be between 0.29-1.81
527 m by 2300, and 0.37-2.77 m by 2500 (Church et al., 2013). We thus expect that the magnitude of
528 oceanographic effects in the HBC will be smaller than the contributions from the Antarctic ice
529 sheet and GIA (Figure 3) but could nonetheless impact the timing of the transition from sea level
530 fall to sea level rise. Incorporating projections of variability in ocean dynamics would add to the
531 work presented here, in addition to improving shorter term projections of sea level and tide
532 changes in the HBC. Furthermore, we have considered changes in sea level and tides in the HBC
533 during the ice-free season. Since Hudson Bay is currently characterized by a long sea ice cover
534 season which dampens the magnitude of the tides (Godin, 1986; Kleptsova & Pietrzak, 2018; St-
535 Laurent et al., 2008), future work will explore the impact of retreating sea ice on our results.
536     Previous simulations of modern tides have had large amplitude errors in the HBC (e.g.
537 Wilmes et al., 2017) due to large uncertainty in the bathymetry in the HBC. Since bathymetry in
538 the HBC is poorly constrained, we used tidal simulations and tide gauge data to constrain the
539 bathymetry. We suggested that being able to simulate tides more accurately provides an
540 indication of which bathymetry dataset is more accurate. We produced a composite bathymetry
541 constrained using TPXO8 solutions and tide gauge observations that greatly improves the fit
542 between predicted and observed modern tides, with total, and deep ocean root mean square errors
543 around 12 and 3 cm, respectively. Our approach may be used to further refine bathymetry
544 models in the Hudson Bay Complex and in other regions with sparse data. Our results also
545 highlight the need for high-resolution bathymetry surveys in the HBC, a region that will become
546 increasingly important as sea ice cover retreats and access via marine traffic increases in a
547 warming climate. Furthermore, accurate bathymetry data has far-reaching implications for
548 residents surrounding the HBC, including, for example, future land claim issues related to the
549 formation of land bridges between islands and the mainland (Tsuji et al., 2016).
550     We emphasize that results from this research have profound impacts on ecosystems and
551 communities surrounding the HBC. Due to the shallow topography and bathymetry in the HBC,
552 we project that an increase in the absolute depth of water of up to 20 % could occur by 2500
553 under our high-end scenario, which would lead to changes in the extent of the intertidal zone and
554 shoreline locations, in turn, affecting ecosystems including wetlands and marshes. If sea level
555 rise outpaces the rate at which marshes grow, these areas will become inundated, reducing the
556 capacity of these ecosystems to attenuate storm surges and flooding events (Kirwan &
557 Guntenspergen, 2010). The substantial changes in dissipation and thus tidal mixing have the
558 potential to impact water structure and biogeochemistry and thus primary and secondary
559 productivity in HBC. Furthermore, the livelihoods, culture, and traditions of indigenous
560 communities surrounding the HBC are inextricably linked to the natural environment. Coastal
561 management and policy decisions should integrate the physical changes presented here. In doing
562 so, these vulnerable groups will be better equipped to deal with future impacts of climate change
563 on coastal regions.

564        We conclude that projections of changes in sea level and ocean tides in the HBC should
565    take into account not only the sea level changes due to ongoing glacial isostatic adjustment from
566    the past deglaciation, but also consider a range of spatially variable sea level change projections
567    arising from land ice loss, in particular in Antarctica. Uncertainty in projections of change in
568    coastal areas in the HBC is dominated by uncertainty in projections of the evolution of the
569    Antarctic ice sheet. As our understanding of the response of Antarctica to climate change
570    improves, so too will our projections of sea level and tide changes in the Arctic.
571

**Acknowledgments, Samples, and Data**

## References

Amante, C. & B.W. Eakins, 2009. ETOPO1 1 Arc-Minute Global Relief Model: Procedures, Data Sources and Analysis. NOAA Technical Memorandum NESDIS NGDC-24. National Geophysical Data Center, NOAA. doi:10.7289/V5C8276M

Arbic, B., & Garrett, C. (2010). A coupled oscillator model of shelf and ocean tides. *Continental Shelf Research*, *30*(6), 564-574. doi: 10.1016/j.csr.2009.07.008

Arbic, B., Karsten, R., & Garrett, C. (2009). On tidal resonance in the global ocean and the back-effect of coastal tides upon open-ocean tides. *Atmosphere-Ocean*, *47*(4), 239-266. doi: 10.3137/oc311.2009

Arbic, B., MacAyeal, D., Mitrovica, J., & Milne, G. (2004). Ocean tides and Heinrich events. *Nature*, *432*(7016), 460-460. doi: 10.1038/432460a

Arbic, B., St-Laurent, P., Sutherland, G., & Garrett, C. (2007). On the resonance and influence of the tides in Ungava Bay and Hudson Strait. *Geophysical Research Letters*, *34*(17). doi: 10.1029/2007gl030845

Argus, D., Peltier, W., Drummond, R., & Moore, A. (2014). The Antarctica component of postglacial rebound model ICE-6G_C (VM5a) based on GPS positioning, exposure age dating of ice thicknesses, and relative sea level histories. *Geophysical Journal International*, *198*(1), 537-563. doi: 10.1093/gji/ggu140

Becker, J., Sandwell, D., Smith, W., Braud, J., Binder, B., & Depner, J. et al. (2009). Global Bathymetry and Elevation Data at 30 Arc Seconds Resolution: SRTM30_PLUS. *Marine Geodesy*, *32*(4), 355-371. doi: 10.1080/01490410903297766

Carless, S., Green, J., Pelling, H., & Wilmes, S. (2016). Effects of future sea-level rise on tidal processes on the Patagonian Shelf. *Journal Of Marine Systems*, *163*, 113-124. doi: 10.1016/j.jmarsys.2016.07.007

Chen, X., Zhang, X., Church, J., Watson, C., King, M., & Monselesan, D. et al. (2017). The increasing rate of global mean sea-level rise during 1993–2014. *Nature Climate Change*, *7*(7), 492-495. doi: 10.1038/nclimate3325

Church, J.A., P.U. Clark, A. Cazenave, J.M. Gregory, S. Jevrejeva, A. Levermann, M.A. Merrifield, G.A. Milne, R.S. Nerem, P.D. Nunn, A.J. Payne, W.T. Pfeffer, D. Stammer and A.S. Unnikrishnan, 2013: Sea Level Change. In: Climate Change 2013: The Physical Science Basis. Contribution of Working Group I to the Fifth Assessment Report of the Intergovernmental Panel on Climate Change [Stocker, T.F., D. Qin, G.-K. Plattner, M. Tignor, S.K. Allen, J. Boschung, A. Nauels, Y. Xia, V. Bex and P.M. Midgley (eds.)]. Cambridge University Press, Cambridge, United Kingdom and New York, NY, USA.

Clark, J., & Lingle, C. (1977). Future sea-level changes due to West Antarctic ice sheet fluctuations. *Nature*, *269*(5625), 206-209. doi: 10.1038/269206a0

624 Clark, P., Church, J., Gregory, J., & Payne, A. (2015). Recent Progress in Understanding and
625      Projecting Regional and Global Mean Sea Level Change. *Current Climate Change*
626      *Reports*, *1*(4), 224-246. doi: 10.1007/s40641-015-0024-4

627 Clark, P., Shakun, J., Marcott, S., Mix, A., Eby, M., & Kulp, S. et al. (2016). Consequences of
628      twenty-first-century policy for multi-millennial climate and sea-level change. *Nature*
629      *Climate Change*, *6*(4), 360-369. doi: 10.1038/nclimate2923

630 Clarke, A., & Battisti, D. (1981). The effect of continental shelves on tides. *Deep Sea Research*
631      *Part A. Oceanographic Research Papers*, *28*(7), 665-682. doi: 10.1016/0198-
632      0149(81)90128-x

633 Collins, M., R. Knutti, J. Arblaster, J.-L. Dufresne, T. Fichefet, P. Friedlingstein, X. Gao, W.J.
634      Gutowski, T. Johns, G. Krinner, M. Shongwe, C. Tebaldi, A.J. Weaver and M. Wehner,
635      2013: Long-term Climate Change: Projections, Commitments and Irreversibility. In:
636      Climate Change 2013: The Physical Science Basis. Contribution of Working Group I to the
637      Fifth Assessment Report of the Intergovernmental Panel on Climate Change [Stocker, T.F.,
638      D. Qin, G.-K. Plattner, M. Tignor, S.K. Allen, J. Boschung, A. Nauels, Y. Xia, V. Bex and
639      P.M. Midgley (eds.)]. Cambridge University Press, Cambridge, United Kingdom and New
640      York, NY, USA.

641 Craft, C., Clough, J., Ehman, J., Joye, S., Park, R., & Pennings, S. et al. (2009). Forecasting the
642      effects of accelerated sea-level rise on tidal marsh ecosystem services. *Frontiers In Ecology*
643      *And The Environment*, *7*(2), 73-78. doi: 10.1890/070219

644 Cummins, P. F., Karsten, R. H. & Arbic, B. K. (2010). The semi-diurnal tide in Hudson strait as
645      a resonant channel oscillation. *Atmosphere-Ocean*, *48*(3), 163-176. doi:
646      10.3137/OC307.2010

647 DeConto, R., & Pollard, D. (2016). Contribution of Antarctica to past and future sea-level
648      rise. *Nature*, *531*(7596), 591-597. doi: 10.1038/nature17145

649 Drinkwater, K. (1986). Chapter 13 Physical Oceanography of Hudson Strait and Ungava Bay.
650      *Canadian Inland Seas*, 237-264. doi: 10.1016/s0422-9894(08)70906-1

651 Dziewonski, A., & Anderson, D. (1981). Preliminary reference Earth model. *Physics Of The*
652      *Earth And Planetary Interiors*, *25*(4), 297-356. doi: 10.1016/0031-9201(81)90046-7

653 Egbert, G., Bennett, A., & Foreman, M. (1994). TOPEX/POSEIDON tides estimated using a
654      global inverse model. *Journal of Geophysical Research*, *99*(C12), 24821. doi:
655      10.1029/94jc01894

656 Egbert, G., & Erofeeva, S. (2002). Efficient Inverse Modeling of Barotropic Ocean
657      Tides. *Journal Of Atmospheric And Oceanic Technology*, *19*(2), 183-204. doi:
658      10.1175/1520-0426(2002)019<0183:eimobo>2.0.co;2

659 Egbert, G., & Ray, R. (2001). Estimates of M2 tidal energy dissipation from TOPEX/Poseidon
660      altimeter data. *Journal Of Geophysical Research: Oceans*, *106*(C10), 22475-22502. doi:
661      10.1029/2000jc000699

662 Egbert, G., Ray, R., & Bills, B. (2004). Numerical modeling of the global semidiurnal tide in the
663      present day and in the last glacial maximum. *Journal Of Geophysical Research:*
664      *Oceans*, *109*(C3). doi: 10.1029/2003jc001973

665 Godin, G. (1986). Modification by an Ice Cover of the Tide in James Bay and Hudson
666      Bay. *ARCTIC*, *39*(1). doi: 10.14430/arctic2048

667 Golledge, N., Keller, E., Gomez, N., Naughten, K., Bernales, J., Trusel, L., & Edwards, T.
668      (2019). Global environmental consequences of twenty-first-century ice-sheet
669      melt. *Nature*, *566*(7742), 65-72. doi: 10.1038/s41586-019-0889-9

670 Golledge, N., Kowalewski, D., Naish, T., Levy, R., Fogwill, C., & Gasson, E. (2015). The multi-
671      millennial Antarctic commitment to future sea-level rise. *Nature*, *526*(7573), 421-425. doi:
672      10.1038/nature15706

673 Gomez, N., Mitrovica, J., Tamisiea, M., & Clark, P. (2010). A new projection of sea level
674      change in response to collapse of marine sectors of the Antarctic Ice Sheet. *Geophysical*
675      *Journal International*, *180*(2), 623-634. doi: 10.1111/j.1365-246x.2009.04419.x

676 Gough, W.A. 1998. Projections of sea-level change in Hudson and James Bays, Canada, due to
677      global warming. Arctic and Alpine Research 30(1):84 – 88. doi: 10.2307/1551748

678 Green, J. (2010). Ocean tides and resonance. *Ocean Dynamics*, *60*(5), 1243-1253. doi:
679      10.1007/s10236-010-0331-1

680 Green, J., & Nycander, J. (2013). A Comparison of Tidal Conversion Parameterizations for Tidal
681      Models. *Journal Of Physical Oceanography*, *43*(1), 104-119. doi: 10.1175/jpo-d-12-023.1

682 Hay, C., Morrow, E., Kopp, R., & Mitrovica, J. (2015). Probabilistic reanalysis of twentieth-
683      century sea-level rise. *Nature*, *517*(7535), 481-484. doi: 10.1038/nature14093

684 Harker, A., Green, J. A. M., Schindelegger, M., & Wilmes, S.-B. (2019). The impact of sea-level
685      rise on tidal characteristics around Australia. *Ocean Science*, *15*, 147–159. doi:/10.5194/os-
686      15-147-2019

687 Idier, D., Paris, F., Cozannet, G., Boulahya, F., & Dumas, F. (2017). Sea-level rise impacts on
688      the tides of the European Shelf. *Continental Shelf Research*, *137*, 56-71. doi:
689      10.1016/j.csr.2017.01.007

690 IPCC (2014). Climate Change 2014: Impacts, Adaptation, and Vulnerability. Summaries,
691      Frequently Asked Questions, and Cross-Chapter Boxes. A Contribution of Working Group
692      II to the Fifth Assessment Report of the Intergovernmental Panel on Climate Change [Field,
693      C.B., V.R. Barros, D.J. Dokken, K.J. Mach, M.D. Mastrandrea, T.E. Bilir, M. Chatterjee,
694      K.L. Ebi, Y.O. Estrada, R.C. Genova, B. Girma, E.S. Kissel, A.N. Levy, S.
695      MacCracken,P.R. Mastrandrea, and L.L. White (eds.)]. World Meteorological Organization,
696      Geneva, Switzerland, 190 pp.

697 IPCC (2019). Special Report on the Ocean and Cryosphere in a Changing Climate
698      (SROCC) (2019); www.ipcc.ch/report/srocc.

699  Jevrejeva, S., Jackson, L., Riva, R., Grinsted, A., & Moore, J. (2016). Coastal sea level rise with
700      warming above 2 °C. *Proceedings of The National Academy Of Sciences*, *113*(47), 13342-
701      13347. doi: 10.1073/pnas.1605312113

702  Kendall, R., Mitrovica, J., & Milne, G. (2005). On post-glacial sea level - II. Numerical
703      formulation and comparative results on spherically symmetric models. *Geophysical Journal
704      International*, *161*(3), 679-706. doi: 10.1111/j.1365-246x.2005.02553.x

705  Kirwan, M., & Guntenspergen, G. (2010). Influence of tidal range on the stability of coastal
706      marshland. *Journal of Geophysical Research: Earth Surface*, *115*(F2). doi:
707      10.1029/2009jf001400

708  Kirwan, M., & Megonigal, J. (2013). Tidal wetland stability in the face of human impacts and
709      sea-level rise. *Nature*, *504*(7478), 53-60. doi: 10.1038/nature12856

710  Kirwan, M., Guntenspergen, G., D'Alpaos, A., Morris, J., Mudd, S., & Temmerman, S. (2010).
711      Limits on the adaptability of coastal marshes to rising sea level. *Geophysical Research
712      Letters*, *37*(23), n/a-n/a. doi: 10.1029/2010gl045489

713  Kleptsova, O., & Pietrzak, J. (2018). High resolution tidal model of Canadian Arctic
714      Archipelago, Baffin and Hudson Bay. *Ocean Modelling*, *128*, 15-47. doi:
715      10.1016/j.ocemod.2018.06.001

716  Kopp, R., DeConto, R., Bader, D., Hay, C., Horton, R., & Kulp, S. et al. (2017). Evolving
717      Understanding of Antarctic Ice-Sheet Physics and Ambiguity in Probabilistic Sea-Level
718      Projections. *Journal of Geophysical Research: Earth's Future*, *5*(12), 1217-1233. doi:
719      10.1002/2017ef000663

720  Lemmen, D.S. and Warren, F.J. (2016): Synthesis; *in* Canada's Marine Coasts in a Changing
721      Climate, (ed.) D.S. Lemmen, F.J. Warren, T.S. James and C.S.L. Mercer Clarke;
722      Government of Canada, Ottawa, ON, p. 17-26.

723  Mitrovica, J., Gomez, N., Morrow, E., Hay, C., Latychev, K., & Tamisiea, M. (2011). On the
724      robustness of predictions of sea level fingerprints. *Geophysical Journal
725      International*, *187*(2), 729-742. doi: 10.1111/j.1365-246x.2011.05090.x

726  Mitrovica, J., Tamisiea, M., Davis, J., & Milne, G. (2001). Recent mass balance of polar ice
727      sheets inferred from patterns of global sea-level change. *Nature*, *409*(6823), 1026-1029. doi:
728      10.1038/35059054

729  Nerem, R., Beckley, B., Fasullo, J., Hamlington, B., Masters, D., & Mitchum, G. (2018).
730      Climate-change–driven accelerated sea-level rise detected in the altimeter era. *Proceedings
731      of The National Academy of Sciences*, *115*(9), 2022-2025. doi: 10.1073/pnas.1717312115

732  Nicholls, R., & Cazenave, A. (2010). Sea-Level Rise and Its Impact on Coastal
733      Zones. *Science*, *328*(5985), 1517-1520. doi: 10.1126/science.1185782

734  O'Reilly, C. T., R. Solvason, and C. Solomon (2005), Where are the world's largest tides?, in
735      BIO Annual Report ''2004 in Review,'' edited by J. Ryan, pp. 44 – 46, Biotechnol. Ind.
736      Org., Washington, D. C.

737 Padman, L., Siegfried, M., & Fricker, H. (2018). Ocean Tide Influences on the Antarctic and
738     Greenland Ice Sheets. *Reviews of Geophysics*, *56*(1), 142-184. doi: 10.1002/2016rg000546

739 Passeri, D., Hagen, S., Plant, N., Bilskie, M., Medeiros, S., & Alizad, K. (2016). Tidal
740     hydrodynamics under future sea level rise and coastal morphology in the Northern Gulf of
741     Mexico. *Journal Geophysical Research: Earth's Future*, *4*(5), 159-176. doi:
742     10.1002/2015ef000332

743 Pelling, H., & Green, J. (2013). Sea level rise and tidal power plants in the Gulf of
744     Maine. *Journal Of Geophysical Research: Oceans*, *118*(6), 2863-2873. doi:
745     10.1002/jgrc.20221

746 Pelling, H., & Green, J. (2014). Impact of flood defences and sea-level rise on the European
747     Shelf tidal regime. *Continental Shelf Research*, 85, 96-105. doi: 10.1016/j.csr.2014.04.011

748 Pelling, H., Green, J., & Ward, S. (2013). Modelling tides and sea-level rise: To flood or not to
749     flood. *Ocean Modelling*, *63*, 21-29. doi: 10.1016/j.ocemod.2012.12.004

750 Pelling, H., Uehara, K., & Green, J. (2013). The impact of rapid coastline changes and sea level
751     rise on the tides in the Bohai Sea, China. *Journal Of Geophysical Research: Oceans*, *118*(7),
752     3462-3472. doi: 10.1002/jgrc.20258

753 Peltier, W. (2004). Global glacial isostasy and the surface of the ice-age Earth: the ICE-5G
754     (VM2) model and GRACE. *Annual Review of Earth and Planetary Sciences*, *32*(1), 111-
755     149. doi: 10.1146/annurev.earth.32.082503.144359

756 Peltier, W., Argus, D., & Drummond, R. (2015). Space geodesy constrains ice age terminal
757     deglaciation: The global ICE-6G_C (VM5a) model. *Journal of Geophysical Research: Solid
758     Earth*, *120*(1), 450-487. doi: 10.1002/2014jb011176

759 Pickering, M., Wells, N., Horsburgh, K., & Green, J. (2012). The impact of future sea-level rise
760     on the European Shelf tides. *Continental Shelf Research*, *35*, 1-15. doi:
761     10.1016/j.csr.2011.11.011

762 Pollard, D., Gomez, N., & Deconto, R. (2017). Variations of the Antarctic Ice Sheet in a Coupled
763     Ice Sheet-Earth-Sea Level Model: Sensitivity to Viscoelastic Earth Properties. *Journal of
764     Geophysical Research: Earth Surface*, *122*(11), 2124-2138. doi: 10.1002/2017jf004371

765 Ross, A., Najjar, R., Li, M., Lee, S., Zhang, F., & Liu, W. (2017). Fingerprints of Sea Level Rise
766     on Changing Tides in the Chesapeake and Delaware Bays. *Journal of Geophysical
767     Research: Oceans*, *122*(10), 8102-8125. doi: 10.1002/2017jc012887

768 Slangen, A., Adloff, F., Jevrejeva, S., Leclercq, P., Marzeion, B., Wada, Y., & Winkelmann, R.
769     (2016). A Review of Recent Updates of Sea-Level Projections at Global and Regional
770     Scales. *Surveys in Geophysics*, *38*(1), 385-406. doi: 10.1007/s10712-016-9374-2

771 Stammer, D., Ray, R., Andersen, O., Arbic, B., Bosch, W., & Carrère, L. et al. (2014). Accuracy
772     assessment of global barotropic ocean tide models. *Reviews of Geophysics*, *52*(3), 243-282.
773     doi: 10.1002/2014rg000450

774 Stewart, D.B., and Lockhart, W.L. (2005). *An Overview of the Hudson Bay Marine Ecosystem.*
775     Canadian technical report of fisheries and aquatic sciences no. 2586. Retrieved from
776     Government of Canada, Department of Fisheries and Oceans website: http://www.dfo-
777     mpo.gc.ca/libraries- bibliotheques/toc-tdm/314704-eng.htm

778 St-Laurent, P., Saucier, F., & Dumais, J. (2008). On the modification of tides in a seasonally ice-
779     covered sea. *Journal of Geophysical Research*, *113*(C11). doi: 10.1029/2007jc004614

780 Tamisiea, M., & Mitrovica, J. (2011). The Moving Boundaries of Sea Level Change:
781     Understanding the Origins of Geographic Variability. *Oceanography*, *24*(2), 24-39. doi:
782     10.5670/oceanog.2011.2

783 Tsuji, L.J.S., Gomez, N., Mitrovica, J.X., and Kendall, R. (2009). Post-glacial isostatic
784     adjustment and global warming in Subarctic Canada: Implications for islands of the James
785     Bay region. Arctic 62(4):458 – 467. doi: 10.14430/arctic176

786 Tsuji, L., Daradich, A., Gomez, N., Hay, C., & Mitrovica, J. (2016). Sea Level Change in the
787     Western James Bay Region of Subarctic Ontario: Emergent Land and Implications for
788     Treaty No. 9. Arctic, 69(1), 99. doi: 10.14430/arctic4542

789 Uehara, K., Scourse, J., Horsburgh, K., Lambeck, K., & Purcell, A. (2006). Tidal evolution of
790     the northwest European shelf seas from the Last Glacial Maximum to the present. *Journal*
791     *Of Geophysical Research*, *111*(C9). doi: 10.1029/2006jc003531

792 Weatherall, P., Marks, K., Jakobsson, M., Schmitt, T., Tani, S., & Arndt, J. et al. (2015). A new
793     digital bathymetric model of the world's oceans. *Earth and Space Science*, *2*(8), 331-345.
794     doi: 10.1002/2015ea000107

795 Webb, D. (2014). On the tides and resonances of Hudson Bay and Hudson Strait. *Ocean*
796     *Science*, *10*(3), 411-426. doi: 10.5194/os-10-411-2014

797 Wilmes, S., Green, J., Gomez, N., Rippeth, T., & Lau, H. (2017). Global Tidal Impacts of Large-
798     Scale Ice Sheet Collapses. *Journal of Geophysical Research: Oceans*, *122*(11), 8354-8370.
799     doi: 10.1002/2017jc013109

800 Winkelmann, R., Martin, M., Haseloff, M., Albrecht, T., Bueler, E., Khroulev, C., & Levermann,
801     A. (2011). The Potsdam Parallel Ice Sheet Model (PISM-PIK) – Part 1: Model
802     description. *The Cryosphere*, *5*(3), 715-726. doi: 10.5194/tc-5-715-2011

803 Woodward, R. (1888), On the form of and position of mean sea level, *U.S. Geol. Surv. Bull.*, 48,
804     87–170.

805 WRCP Global Sea Level Budget Group. Global sea-level budget 1993–present. (2018). *Earth*
806     *System Science Data*, *10*(3), 1551-1590. doi: 10.5194/essd-10-1551-2018

807
808
809
810
811

|  | $M_2$ | $S_2$ | $K_1$ |
|---|---|---|---|
| **ETOPO1** | 70.7 / 36.7 / 38.3 | 25 / 10.8 / 11.8 | 4.7 / 3.2 / 4.0 |
| - **HB** | 39.2 | 12.7 | 3.6 |
| - **HS/FB/CS** | 127.8 | 47.1 | 6.5 |
| **SRTM** | 50.2 / 33.9 / 37.8 | 22.2 / 10.3 / 11.6 | 3.9 / 2.8 / **3.3** |
| - **HB** | 56.6 | 20.8 | 4.4 |
| - **HS/FB/CS** | 38.5 | 24.7 | 2.8 |
| **GEBCO 2008** | 54.3 / 24.2 / 25.3 | 17.4 / 8.4 / 9.2 | 3.0 / 3.3 / 4.1 |
| - **HB** | 38.3 | 10.1 | 3.2 |
| - **HB/FB/CS** | 83.3 | 30.4 | 2.5 |
| **GEBCO 2014** | 47.8 / 29.8 / 30.9 | 16.6 / 9.2 / 10.1 | 3.6 / 2.8 / 3.3 |
| - **HB** | 25.8 | **5.7** | 3.4 |
| - **HB/FB/CS** | 87.4 | 36.0 | 3.9 |
| **COMPOSITE** | **19.3 / 14.4 / 15.9** | **11.8 / 4.7 / 5.7** | **2.9 / 2.6** / 3.6 |
| - **HB** | **15.0** | 6.6 | **3.1** |
| - **HS/FB/CS** | **27.0** | **21.2** | **2.4** |

812
813
814 **Table 1:** Bathymetry evaluation. Shown are complex elevation errors in cm between the tide
815 model simulations using the respective bathymetry and tide gauges / TPXO8 / TPXO9 for $M_2$, $S_2$
816 and $K_1$. The best fit has been highlighted for each constituent and evaluation method. For each
817 bathymetry we also show errors against the tide gauges located in Hudson Bay only and the tide
818 gauges located in Hudson Strait (HB), Frobisher Bay (FB) and Cumberland Sound (CS).
819
820 **Figure 1**: Model domain used in this study, showing a) Bathymetry and topography of the
821 Hudson Bay Complex, (data from the composite dataset described in section 3) defined here as
822 Hudson Bay, James Bay, Foxe Basin and Hudson Strait, b) Present day semi-diurnal ($M_2$) tidal
823 amplitudes (colour) and phases (contoured in white lines at 1/8 $M_2$ period), taken from the
824 TPXO8 tide database (http://volkov.oce.orst.edu/tides/tpxo8_atlas.html).
825
826 **Figure 2**: Amplitude differences between simulated $M_2$ amplitudes from several bathymetry
827 datasets and $M_2$ amplitudes from the TPXO8 tidal solution. a) ETOPO1 (Amante & Eakins,
828 2009), b) GEBCO 2008 (http://www.gebco.net), c) SRTM30_Plus (Becker et al., 2009), d)
829 GEBCO 2014 (http://www.gebco.net), e) our new, composite bathymetry with SRTM30_Plus in
830 Hudson Bay and GEBCO 2008 elsewhere. The colored circles show the amplitude differences
831 for the tide-gauge locations (see also Text S1 and Table S4).
832
833 **Figure 3**: Contributions to sea level change in the HBC from GIA and future melting of the polar
834 ice sheets under RCP8.5 at 2100, 2300 and 2500, relative to 2000. Blue shading corresponds to a
835 sea level fall and red shading corresponds to a sea level rise. (a-c) Contribution to sea level
836 change from past ice-ocean loading changes (i.e. GIA) over the last deglaciation associated with
837 the ICE-5G ice history (Peltier, 2004). (d-f) Contribution to sea level change from the Greenland
838 Ice Sheet (Golledge et al., 2019). (g-l) Contribution to sea level change from the Antarctic Ice
839 Sheet under from (g-i) low-end (Golledge et al., 2019) and (j-l) high-end (Pollard et al., 2017)

840      projections. Note the different color scales, the color bar associated with each panel is on the
841      right side of each plot.
842
843      **Figure 4**: Total projected sea level change at 2100, 2300, and 2500, relative to 2000. Sum of
844      individual contributions presented in **Figure 3**. Panels a-c correspond to the low-end Antarctic
845      ice loss scenario (Golledge et al., 2019). Panels d-f correspond to the high-end Antarctic ice loss
846      scenario (Pollard et al., 2017).
847
848      **Figure 5**: Total projected M2 amplitude change at 2100, 2300, and 2500, relative to 2000 for
849      simulations where flooding of low-lying land is permitted with increasing sea levels. Panels a-c
850      correspond to tidal changes associated with the low-end Antarctic ice loss scenario (Golledge et
851      al., 2019). Panels d-f correspond to tidal changes associated with the high-end Antarctic ice loss
852      scenario (Pollard et al., 2017).

**Figure 1.**

**a)**

-400  300  200  100  0  125  425  1000

meters

**b)**

0  0.50  1.00  1.50  2.00  2.50  3.00  3.50

meters

**Figure 2.**

**Figure 3.**
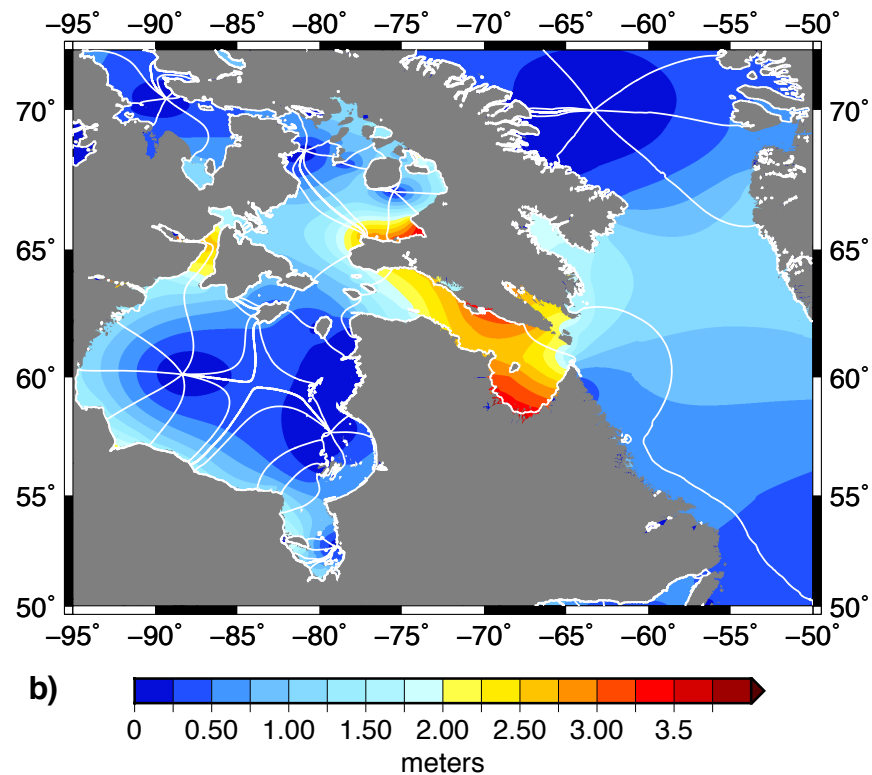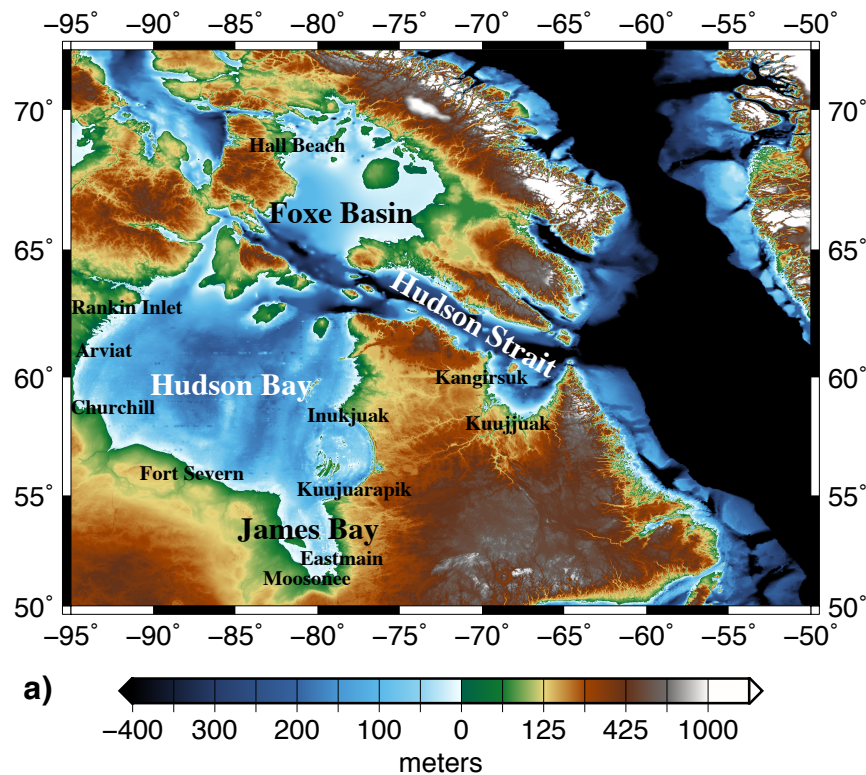
**2100 - 2000**          **2300 - 2000**          **2500 - 2000**
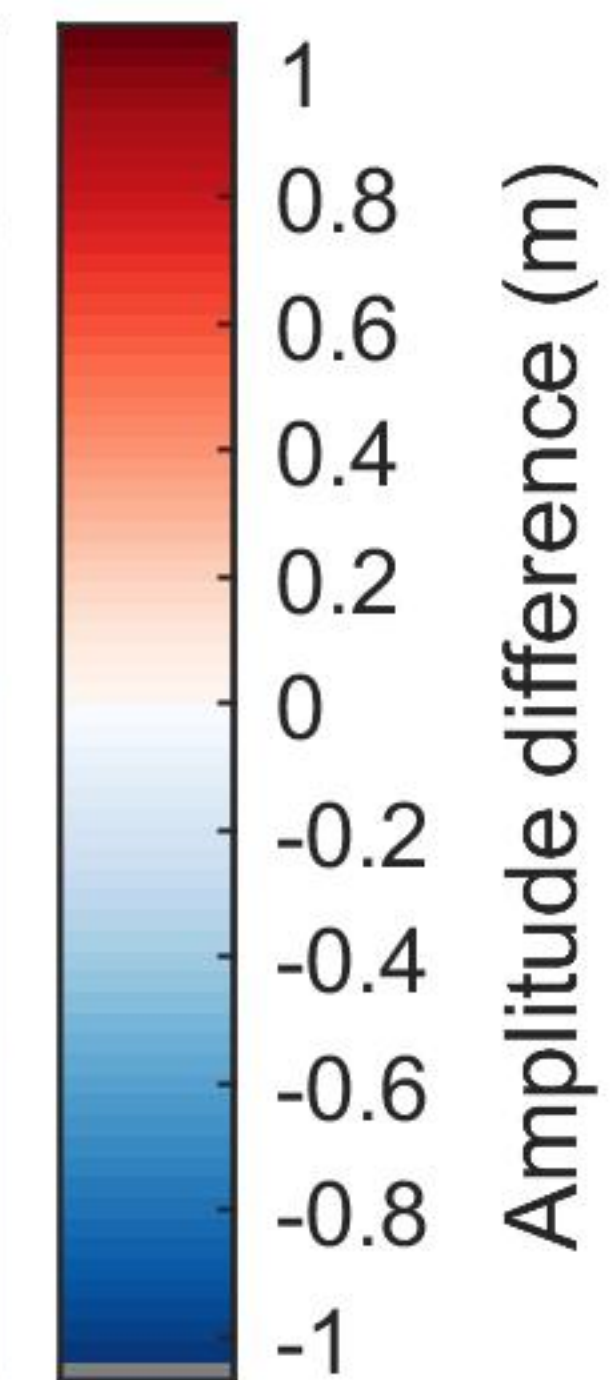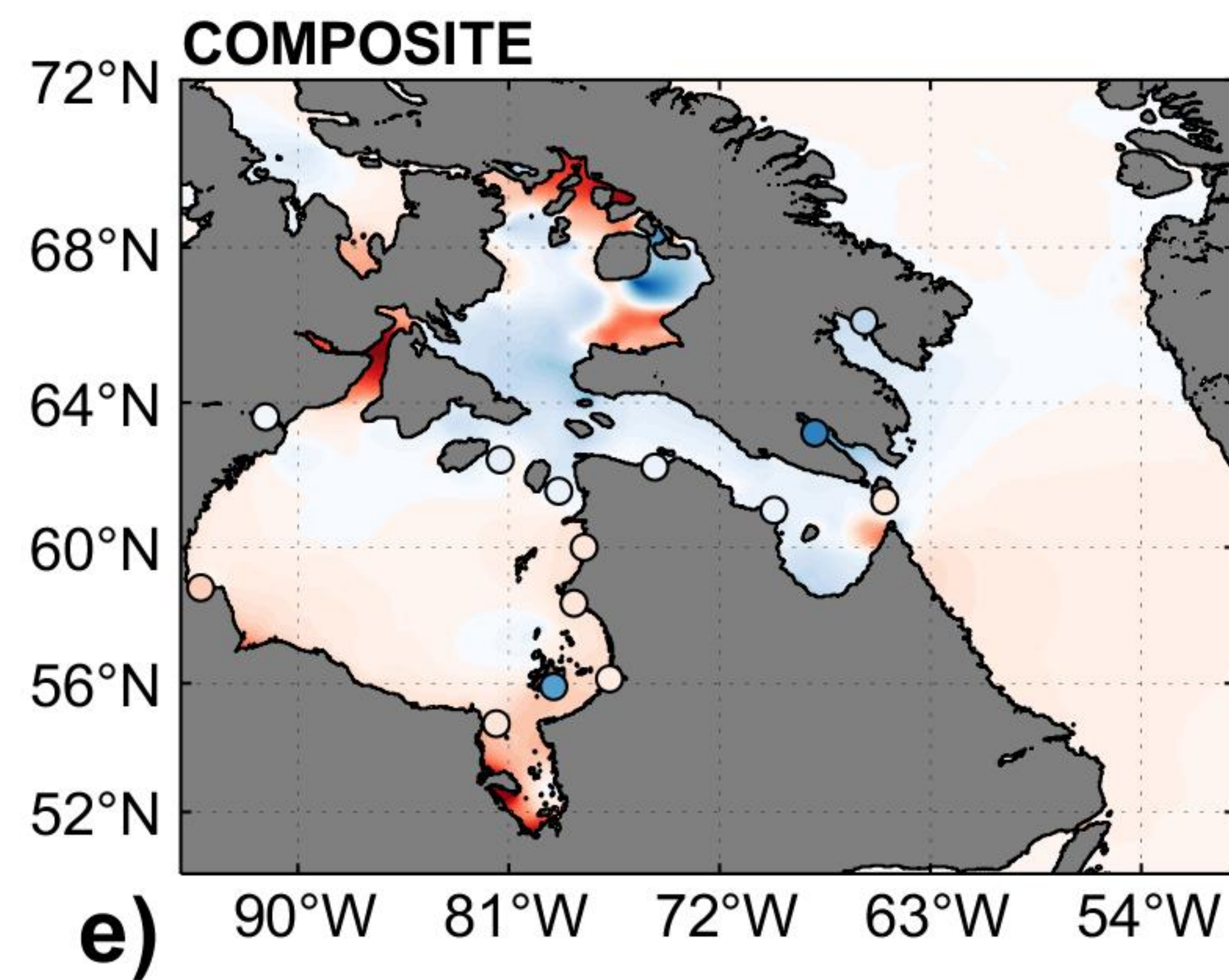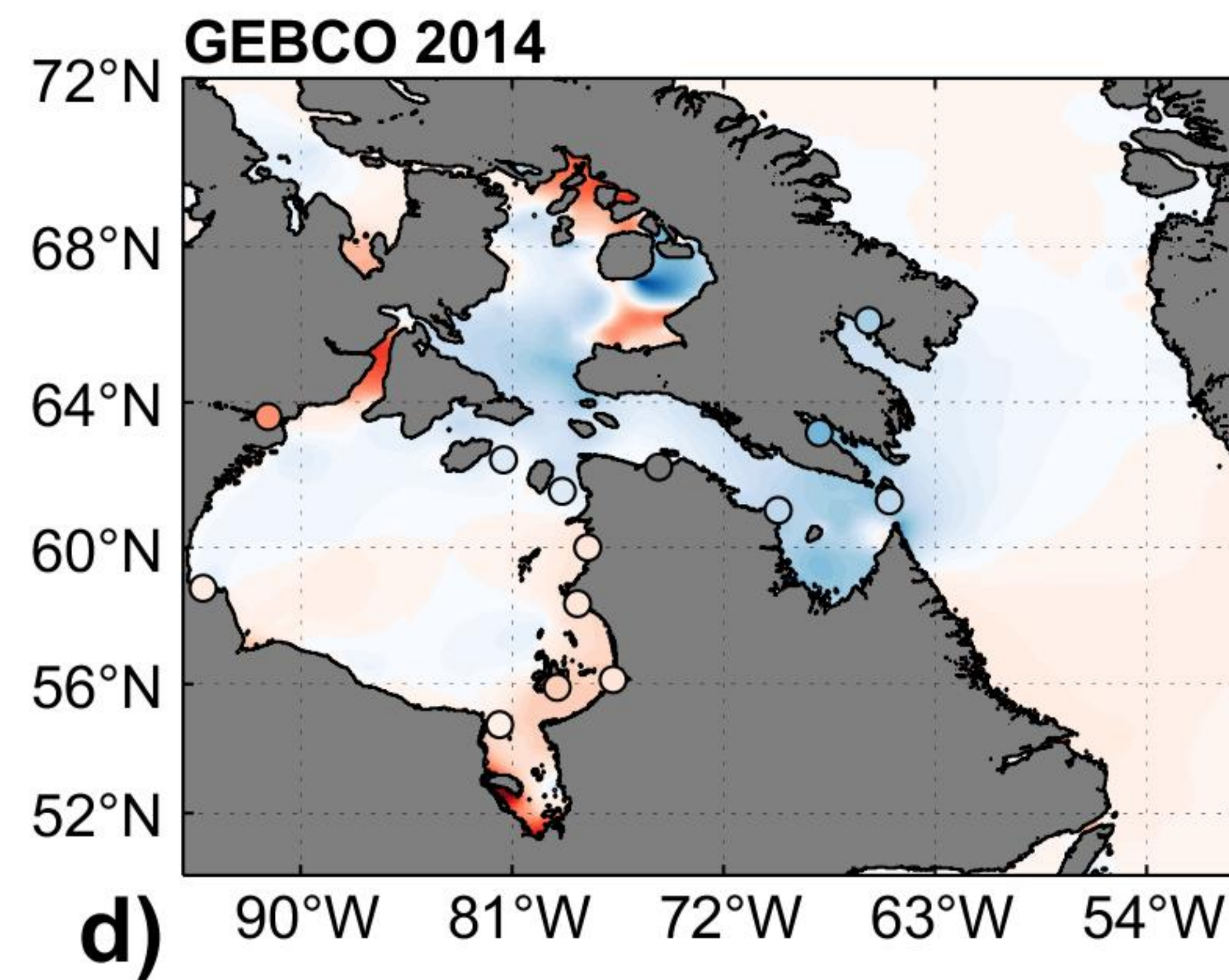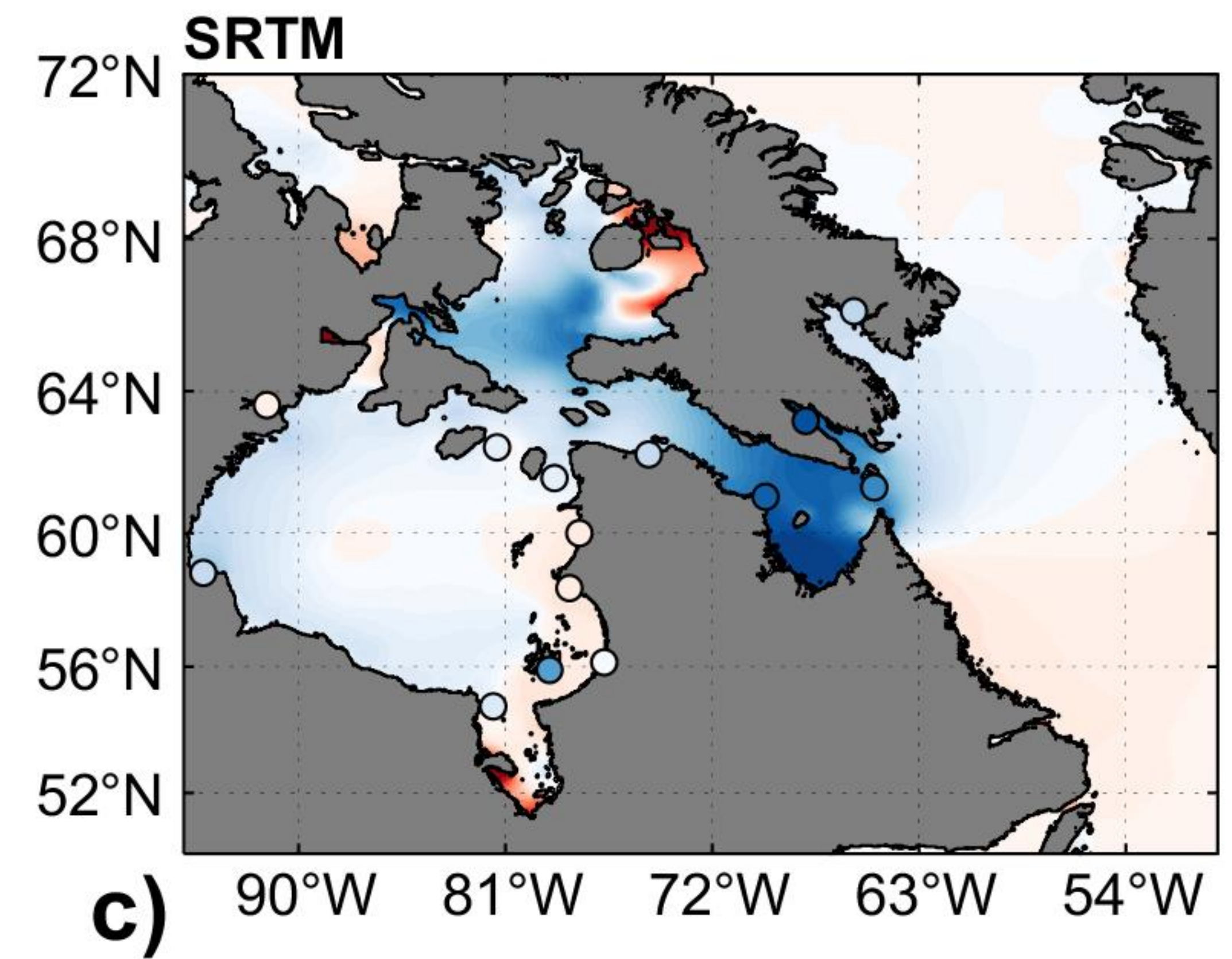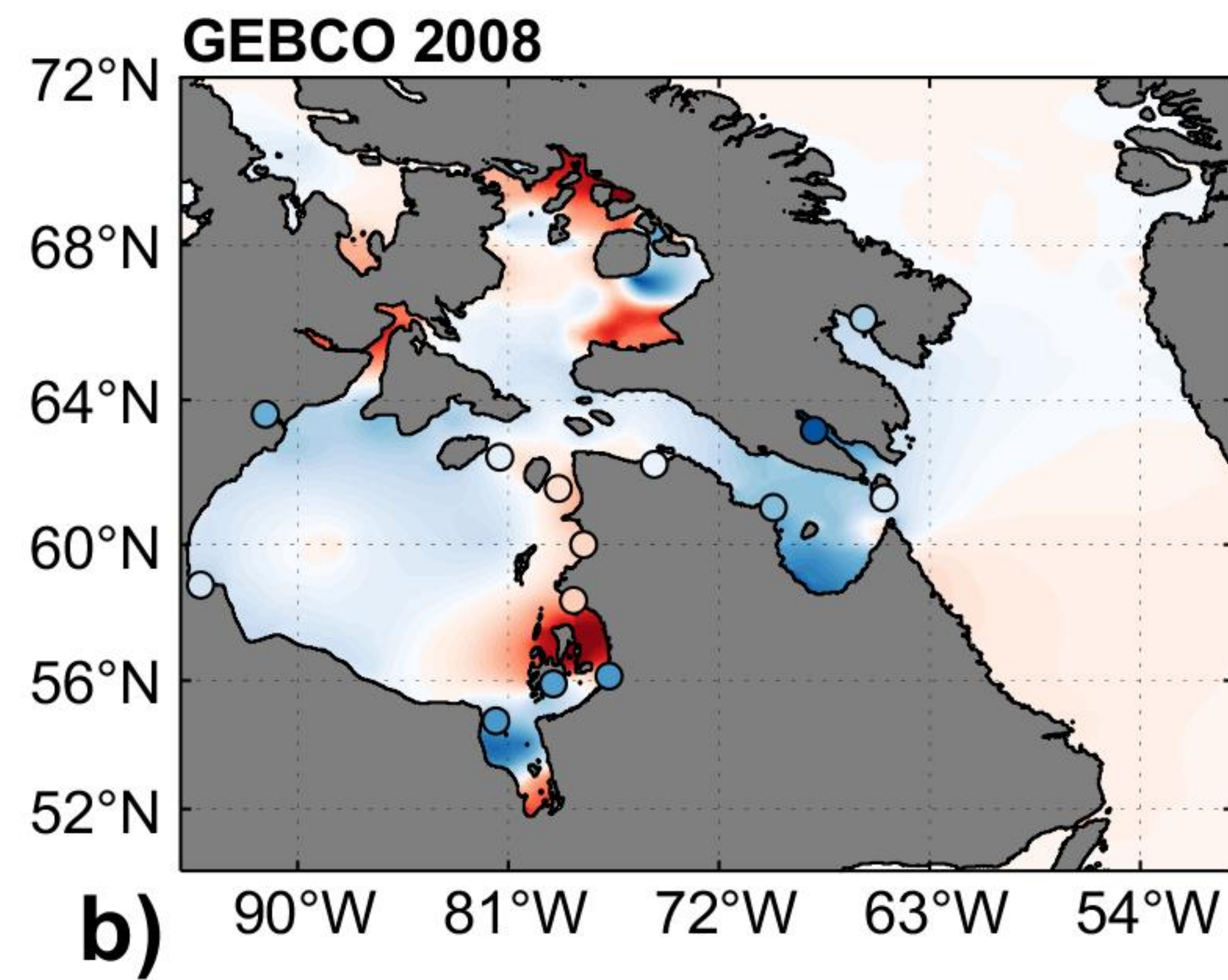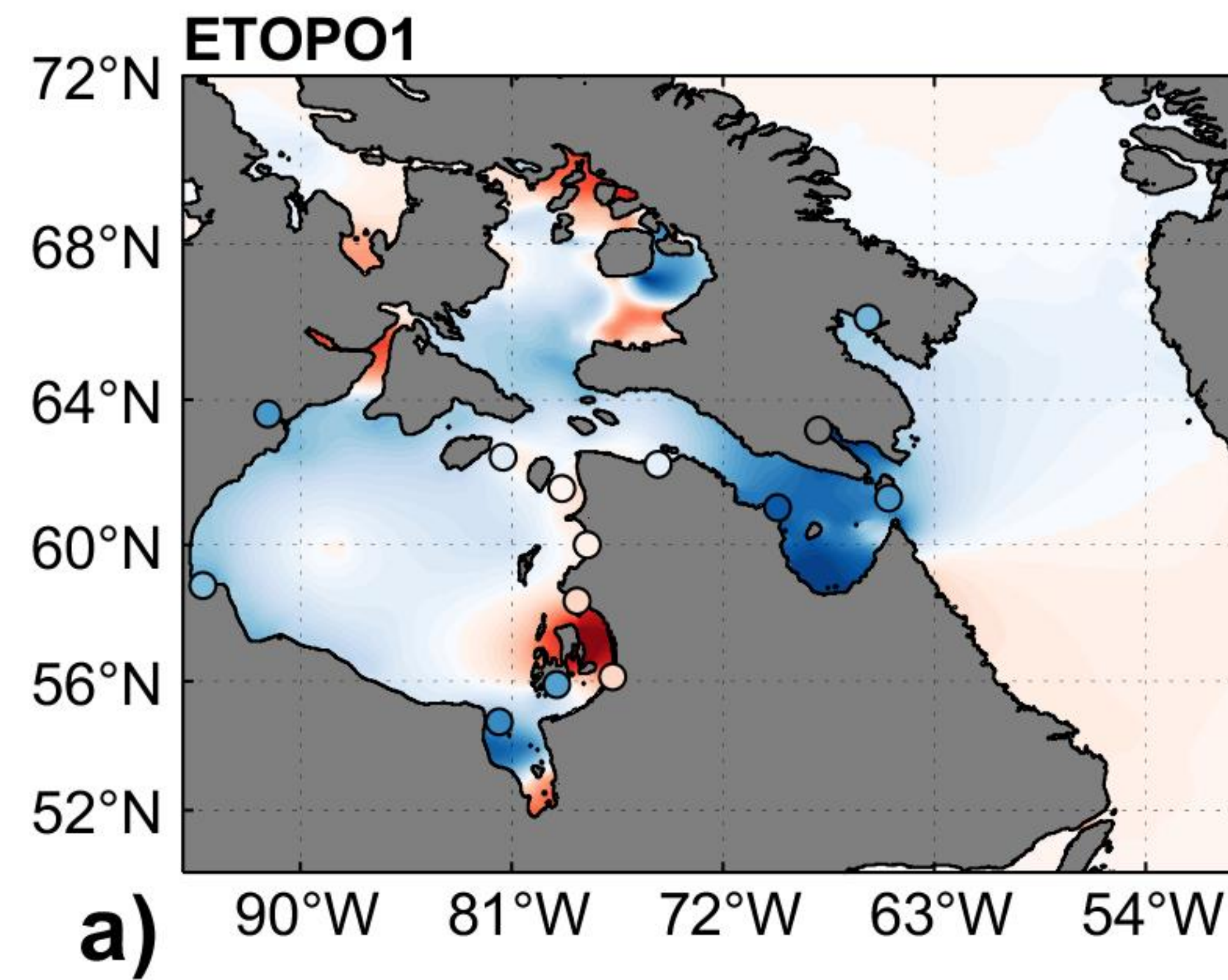
GIA
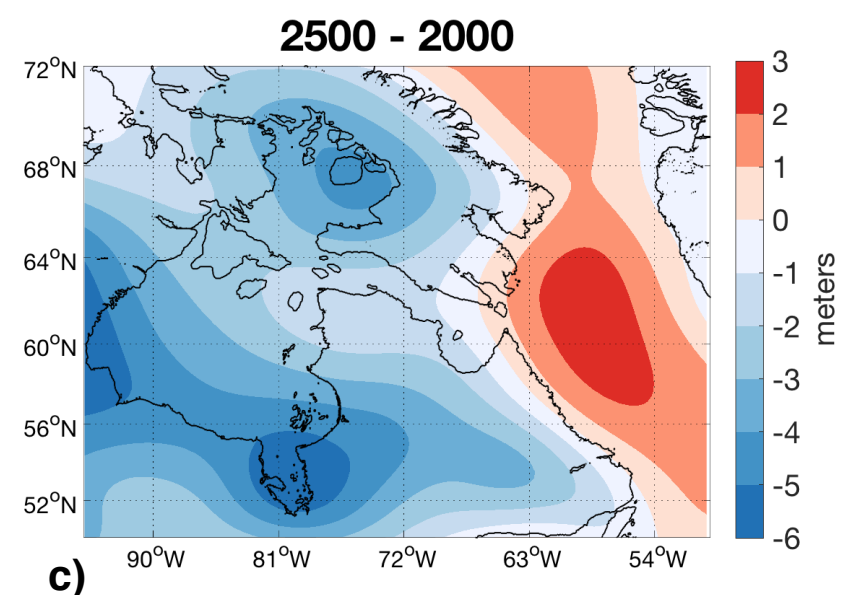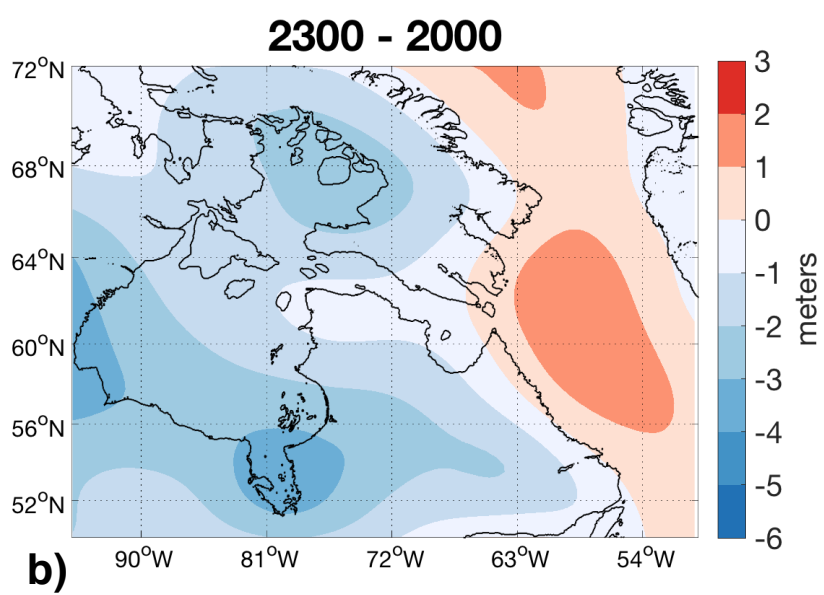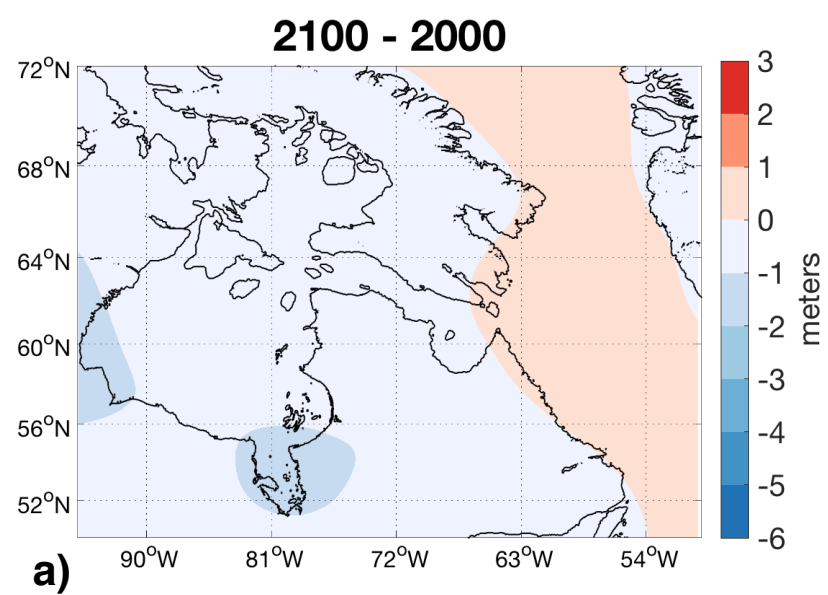
Greenland
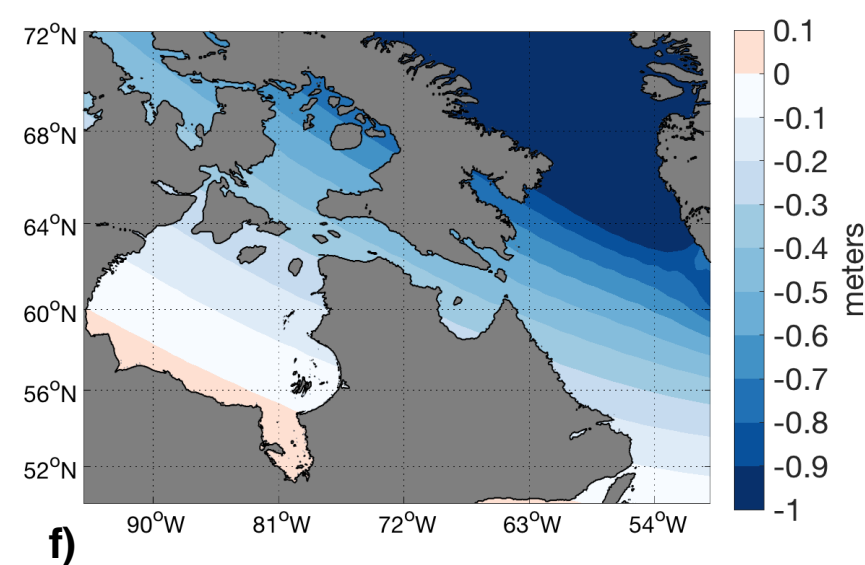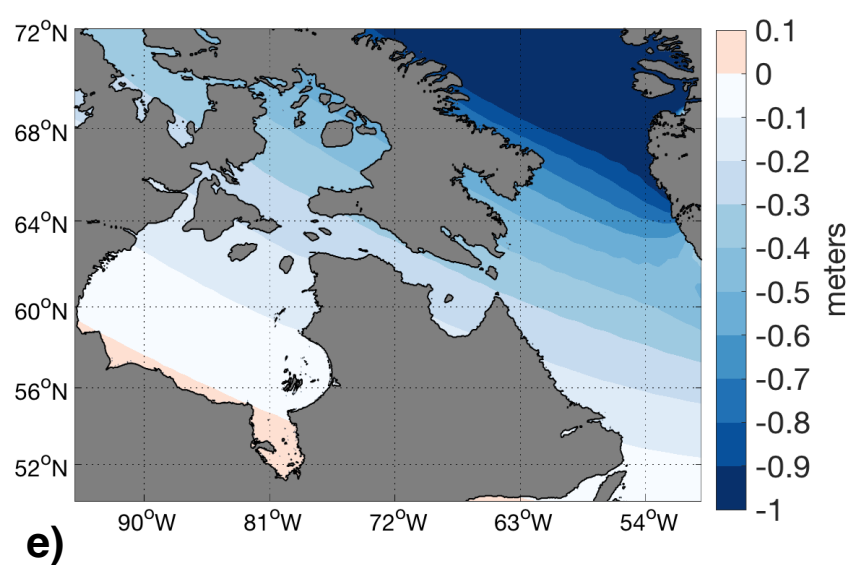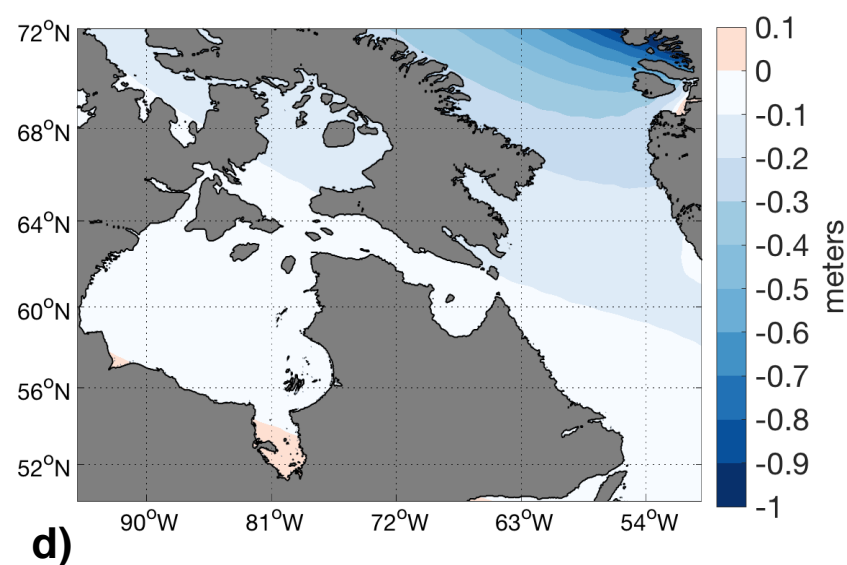
Antarctica low-end

Antarctica high-end

a) b) c) d) e) f) g) h) i) j) k) l)

**Figure 4.**

**Figure 5.**

**2100 - 2000**     **2300 - 2000**     **2500 - 2000**